

Review

Open Access



2D materials and additives: a dual approach to high-performance tin perovskite solar cells

Jun Hyung Kim^{1,2,#}, Du Hyeon Ryu^{1,3,#}, Sang Hyuk Im³, Jaeki Jeong², Chang Eun Song^{1,4}

¹Photoenergy Research Center, Korea Research Institute of Chemical Technology, Daejeon 34114, Republic of Korea.

²Department of Energy Science, Sungkyunkwan University, Suwon 16419, Republic of Korea.

³Department of Chemical and Biological Engineering, Korea University, Seoul 02841, Republic of Korea.

⁴Advanced Materials and Chemical Engineering, University of Science and Technology (UST), Daejeon 34113, Republic of Korea.

[#]They contributed equally to this work.

Correspondence to: Prof. Chang Eun Song, Photoenergy Research Center, Korea Research Institute of Chemical Technology, 141, Gajeong-ro, Yuseong-gu, Daejeon 34114, Republic of Korea. E-mail: songce@kRICT.re.kr; Prof. Jaeki Jeong, Department of Energy Science, Sungkyunkwan University, 25-2, Sungkyunkwan-ro, Jangan-gu, Suwon 16419, Republic of Korea. E-mail: jaeki.jeong@skku.edu; Prof. Sang Hyuk Im, Department of Chemical and Biological Engineering, Korea University, 145 Anam-ro, Seongbuk-gu, Seoul 02841, Republic of Korea. E-mail: imromy@korea.ac.kr

How to cite this article: Kim, J. H.; Ryu, D. H.; Im, S. H.; Jeong, J.; Song, C. E. 2D materials and additives: a dual approach to high-performance tin perovskite solar cells. *Microstructures* 2025, 5, 2025063. <https://dx.doi.org/10.20517/microstructures.2024.192>

Received: 30 Dec 2024 **First Decision:** 22 Feb 2025 **Revised:** 12 Mar 2025 **Accepted:** 24 Mar 2025 **Published:** 8 May 2025

Academic Editor: Sarina Sarina **Copy Editor:** Shu-Yuan Duan **Production Editor:** Shu-Yuan Duan

Abstract

Tin halide perovskite solar cells (THPSCs) are an eco-friendly alternative to lead halide perovskite solar cells. However, defect formation hinders their commercialization. Specifically, the oxidation of Sn^{2+} to Sn^{4+} generates defects, which increase background current due to charge recombination and consequently degrade device performance. This review explores the use of two-dimensional (2D) materials and additives to enhance the performance and stability of THPSCs. 2D materials improve charge transport, passivate defects, induce vertical alignment, and enhance structural stability against moisture. Additives optimize film morphology and interface properties by promoting grain growth and reducing defect density. These approaches increase the power conversion efficiency of THPSCs by up to 15%, demonstrating their commercial potential. The synergistic effects of 2D materials and additives are analyzed, and critical strategies for their combined utilization are suggested to develop high-efficiency and stable THPSCs.

Keywords: Tin halide perovskite, solar cells, 2D materials, additives



© The Author(s) 2025. **Open Access** This article is licensed under a Creative Commons Attribution 4.0 International License (<https://creativecommons.org/licenses/by/4.0/>), which permits unrestricted use, sharing, adaptation, distribution and reproduction in any medium or format, for any purpose, even commercially, as long as you give appropriate credit to the original author(s) and the source, provide a link to the Creative Commons license, and indicate if changes were made.



INTRODUCTION

Organic-inorganic hybrid lead-based perovskites possess excellent optoelectronic properties, such as high absorption coefficients, long carrier diffusion lengths, and a tunable bandgap. These attributes make lead halide perovskite solar cells (LHPSCs) promising candidates for next-generation photovoltaic technologies^[1,2]. These properties arise from the unique electron configuration ($6s^26p^0$) and significant spin-orbit coupling of lead (Pb)^[3]. Recent advances demonstrate an astonishing power conversion efficiency (PCE) exceeding 26%^[4]. Despite these outstanding properties, the commercialization of LHPSCs is hindered by lead toxicity. Researchers are developing various encapsulation technologies to prevent lead leakage, but their long-term effectiveness and reliability require further investigation^[5-7].

To overcome these challenges, various lead-free perovskite solar cells (PSCs) based on bismuth (Bi), germanium (Ge), silver (Ag), and tin (Sn) have been investigated^[8-11]. Among these, tin-based THPSCs have garnered attention due to their similar crystal structure, solar spectrum, and bandgap to LHPSCs without toxicity risk^[12-14]. These superior properties of THPSCs arise from their higher charge mobility, smaller exciton binding energy, and larger Bohr radius than Pb^[15-18]. Tin halide perovskite solar cells (THPSCs) also exhibit high optical absorption coefficients and longer hot-carrier cooling times, which make them promising alternatives^[19,20]. However, THPSCs face challenges such as unfavorable energy band alignment, lattice distortion, and Sn²⁺ oxidation^[21-24]. Easy oxidation of Sn²⁺ leads to instability and poor film quality.

A primary hurdle to realizing high-performance THPSCs is the rapid oxidation of Sn²⁺. Two-dimensional (2D) materials passivate surface defects and control energy levels to enhance charge transfer and stability^[25]. These materials also offer high moisture resistance, compensating for the weak moisture stability of THPSCs. This passivation significantly reduces non-radiative recombination, improves charge extraction, and enhances device efficiency^[26]. Furthermore, 2D materials enable precise control over energy level alignment at the perovskite/charge transport layer interface, thus facilitating efficient charge transfer and minimizing energy losses^[27,28]. This inherent moisture resistance is a key factor for the long-term stability of THPSCs, especially compared to LHPSCs.

Introduced either during the perovskite precursor solution stage or through post-treatment, additives such as metal halides, organic salts, and specific polymers play a vital role alongside 2D materials. They effectively complement the defect passivation provided by 2D materials, with a particularly significant impact on grain boundary defects, major contributors to charge recombination in perovskite films. By further reducing these defects, additives minimize charge recombination losses.

This review explores two key strategies to enhance the performance and stability of THPSCs. These strategies include incorporating 2D materials and additives. While we briefly introduce successful approaches in LHPSCs using 2D materials and additive engineering, this work primarily focuses on their application to THPSCs. In particular, this review highlights the synergistic effects achieved by combining 2D materials and additives in THPSCs. We provide a comprehensive overview of current progress in improving the performance and stability of THPSCs and suggest critical strategies for developing high-efficiency and stable THPSCs.

TIN HALIDE PEROVSKITE SOLAR CELLS: FUNDAMENTALS

Tin halide perovskites have emerged as promising alternatives to lead-based perovskites, offering environmentally friendly and efficient solutions. These materials adopt the general perovskite formula ABX_3 , where A is an organic or inorganic cation such as methylammonium (MA), formamidinium (FA), or cesium (Cs), B is a metal cation Sn, and X is a halide anion I, Br, or Cl^[29-31]. The combination of A-site

cations and X-site halide anions influences the crystal structure, band gap, and overall stability of the material, ultimately determining the performance of perovskite solar cell devices [Figure 1A].

The working mechanism follows the same fundamental principles as conventional LHPSCs and consists of four primary steps. First, electron-hole pairs are generated when the perovskite layer absorbs incident photons. The built-in electric field at the interface between the perovskite and the charge transport layers facilitates the separation of these pairs into free electrons and holes. The separated charge carriers migrate to the electron transport layer (ETL) and hole transport layer (HTL), generating an electric current in the external circuit [Figure 1B]. Perovskite materials are classified into 2D and 3D structures based on the dimensionality of their crystal framework^[32]. 3D perovskites, represented by the formula ABX_3 , exhibit a continuous structure in which BX_6 octahedra share corners to form an extended 3D network^[33]. This configuration facilitates high charge carrier mobility and a well-defined band gap, enabling efficient light absorption and charge transport^[34].

On the other hand, 2D perovskites have a layered structure with large organic spacer cations, improving their stability and moisture resistance^[35]. However, the insulating nature of organic spacers hinders charge transport between perovskite layers, and the relatively wide band gap commonly observed in 2D perovskites limits light absorption, thereby reducing photocurrent generation^[36,37]. Despite these limitations in charge transport and light absorption, the inherent stability of 2D perovskites offers a potential pathway to overcome the Sn^{2+} oxidation problem in 3D perovskites.

2D materials: interfacial engineering and stability enhancement

3D THPSCs have shown promising performance in solar cells. However, they are particularly unstable due to the oxidation of Sn^{2+} by water and oxygen, which is the leading cause of device performance degradation. This instability arises from factors such as the susceptibility of Sn^{2+} to oxidation and the volatility of organic cations in the 3D structure. To address this, researchers have used 2D materials to improve the performance and stability of THPSCs. We discuss the strategies for optimizing these materials, including n-value control and small n-phase suppression. Figure 2 shows how 2D materials can be incorporated into THPSCs to improve performance.

2D Ruddlesden-Popper THPSCs

Generally, 3D perovskites with the ABX_3 crystal structure are unstable due to the hydrophilicity of organic cations^[38-43]. Researchers have been exploring the unique properties of 2D layered perovskite materials to address this issue. One such material is the Ruddlesden-Popper (RP) phase, characterized by stacking adjacent layers in a specific step-like arrangement^[44]. This layered structure, first discovered by Ruddlesden and Popper, is represented by the general chemical formula $A'_2A_{n-1}M_nX_{3n+1}$ ^[45]. This formula is composed of a large monovalent organic cation (A'), a small organic cation (A), a divalent metal cation (M), and a halide anion (X). In these RP perovskites, the A' -site acts as a spacer, forming a significant energy barrier on both sides of the inorganic layer due to its insulating properties.

Hydrophobic organic cations, such as phenethylammonium (PEA), butylammonium (BA), and propylammonium (PA), are commonly employed in RP perovskites. These cations induce preferred crystal orientation and create an energy barrier, effectively hindering moisture penetration^[46-49]. Increasing the n-value in $[MX_6]^{4-}$ octahedral slabs increases the inorganic layers' thickness, reducing quantum confinement effects. This results in a decrease in bandgap and exciton binding energy and an increase in carrier mobility. However, it is important to note that even as the n-value increases significantly, the bandgap of 2D RP perovskites does not ideally converge to that of 3D perovskites due to the inherent structural

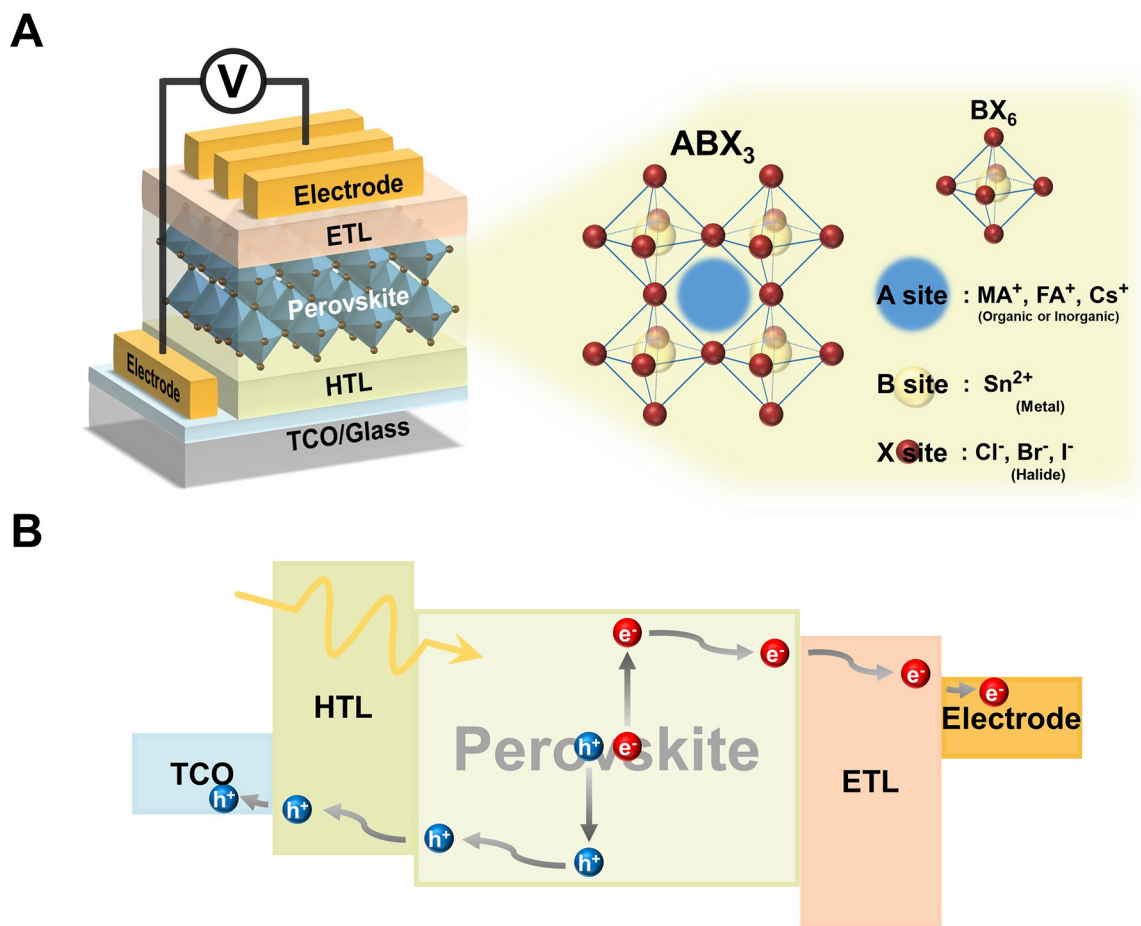


Figure 1. (A) Schematic illustration of three-dimensional (3D) THSPCs; (B) Charge transport mechanism in p-i-n solar cell, illustrating electron-hole pair generation, charge separation, and carrier transport. THSPC: tin halide perovskite solar cell; ETL: electron transport layer; HTL: hole transport layer. TCO: transparent conductive oxide.

differences^[50-53]. While these cations enhance stability, the inherent van der Waals gap in the organic interlayer structure leads to a larger energy bandgap than 3D PSCs. This wider bandgap and other factors like exciton binding energy and charge recombination rates can limit light absorption, particularly in the near-infrared region, and reduce the short-circuit current (J_{sc})^[54,55].

RP THPSCs exhibit optoelectronic performance limitations, including low efficiency, insufficient moisture stability, and high exciton binding energy. Researchers have focused on strategic A'-site modification and n-value engineering. For instance, Kayesh *et al.* investigated the effects of incorporating 5-ammonium valeric acid iodide (5-AVAI) as the organic cation at the A'-site^[56]. They found that 5-AVAI enhanced film uniformity and suppressed Sn^{2+} oxidation by increasing steric hindrance, ultimately improving crystallinity and device stability [Figure 3A].

Beyond A'-site modification, tuning the n-value is crucial for device performance and stability. The n-value in RP perovskites refers to the number of inorganic layers between the organic spacer layers. Increasing the n-value in RP perovskites influences various key properties. Figure 3B demonstrates that tuning the n-value in RP THPSCs ($BA_2MA_{n-1}Sn_nI_{3n+1}$, $n = 2-4$) can optimize optoelectronic properties^[57]. As shown in Figure 3C, the formation energy decreases with an increasing n-value, indicating that 2D perovskites with more layers

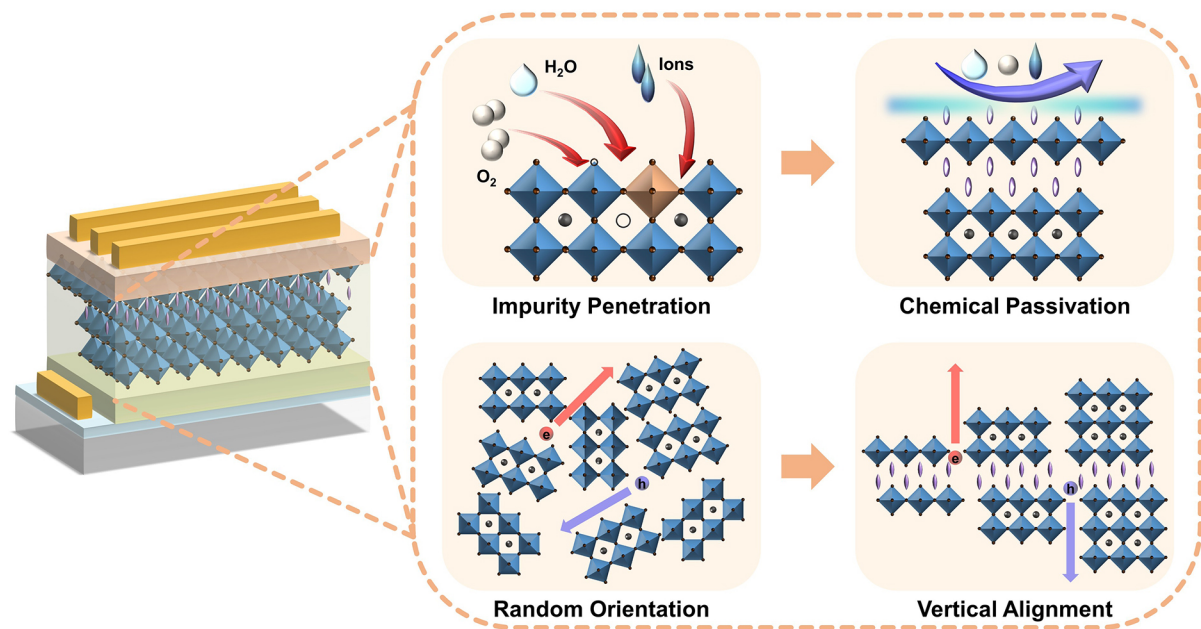


Figure 2. Schematic illustration of how 2D materials enhance performance and stability in 3D THPSCs. THPSC: tin halide perovskite solar cell; 2D: two-dimensional.

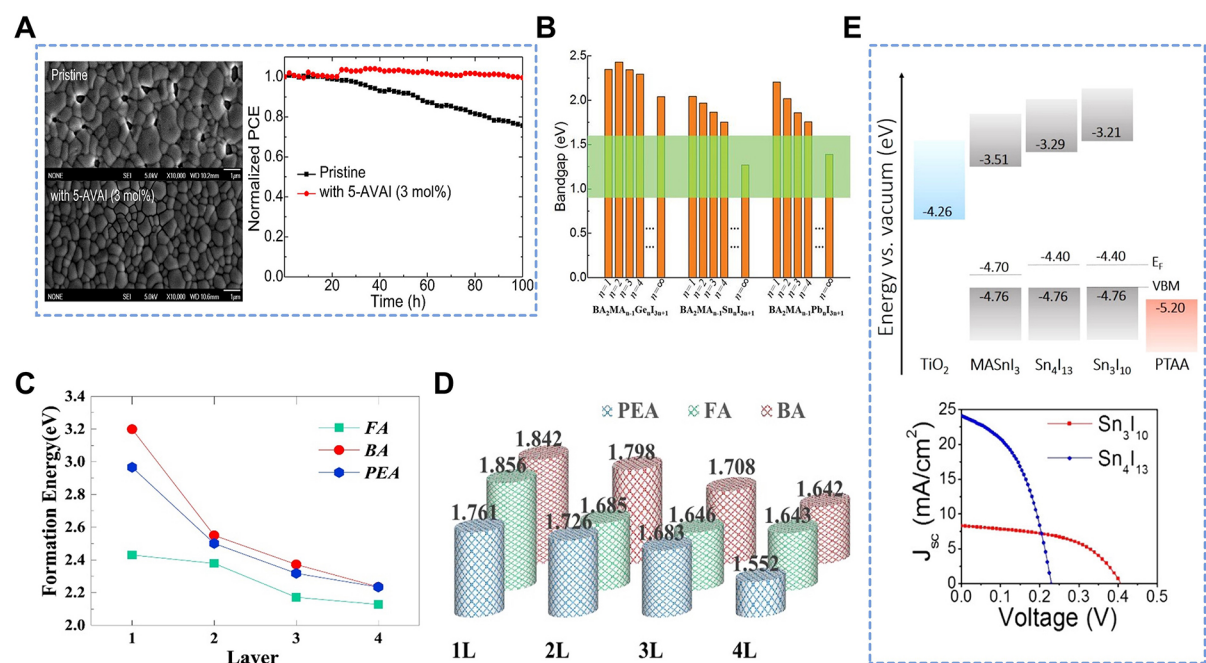


Figure 3. A: SEM images of pristine and 5-AVAI added films (left); Operational stability of encapsulated PSCs with and without 5-AVAI under continuous 1 sun illumination at MPPT (right). This figure is quoted with permission from Kayesh et al. [56]; B: Computed electronic band gaps of $\text{BA}_2\text{MA}_{n-1}\text{MnI}_{3n+1}$ with varying n -values ($M = \text{Ge}, \text{Sn}, \text{and Pb}$) based on the hybrid functional plus SOC scheme. This figure is quoted with permission from MA et al. [57]; C: Formation energies of various functional group clusters are absorbed on layered tin perovskites with different numbers of layers $\text{X}_2(\text{MA})_{n-1}\text{Sn}_n\text{I}_{3n+1}$ ($X = \text{FA}, \text{BA}, \text{PEA}$); D: Calculated HSE06 projected bandgaps of 2D tin perovskites with different numbers of layers and organic cations (L represents the number of layers). This figure is quoted with permission from Wang et al. [58]; E: Schematic illustration of the Band alignment of 3D-MASnI₃, 2D-Sn₄I₁₃, 2D-Sn₃I₁₀ (top), J-V curve of $n = 3$ Sn₃I₁₀ and $n = 4$ Sn₄I₁₃ devices (bottom). This figure is quoted with permission from Cao et al. [59]. PEA: phenethylammonium; BA: butylammonium; PA: propylammonium. SEM: scanning electron microscope; MPPT: maximum power point tracking.

are more stable. Moreover, [Figure 3D](#) illustrates that increasing the n -value leads to a decrease in the bandgap due to quantum confinement effects, demonstrating that the bandgap can be tuned to the optimal range for solar cells (0.9–1.6 eV)^[58]. Cao *et al.* further investigated the influence of the n -value on RP THPSCs. As shown in [Figure 3E](#), adjusting the value leads to higher efficiency due to improved energy level alignment with the TiO₂ electron transport layer and optimized band gap. Notably, 2D perovskites with $n = 4$ exhibits higher efficiency than those with $n = 3$ ^[59]. Suggesting that a synergistic approach combining these strategies could further improve device performance and stability, these studies highlight the importance of A-site modification and n -value engineering in RP THPSCs.

2D Dion-Jacobson THPSCs

The Dion-Jacobson (DJ) phase, characterized by its stacking arrangement of vertically aligned inorganic layers, was first reported by Dion and Jacobson^[44]. This layered structure is represented by the general chemical formula $A'A_{n-1}B_nX_{3n+1}$ ^[60,61]. Unlike RP perovskites, which incorporate monovalent organic cations with a single ammonium group, DJ perovskites utilize divalent organic cations A' with two ammonium groups. This key difference eliminates the van der Waals gap, leading to a reduced interlayer distance and tighter interlayer junction formed through strong hydrogen bonding between the divalent organic cations and adjacent 2D perovskite slabs^[62,63].

DJ perovskites incorporate organic cations like butanediammonium (BDA), 4- (aminomethyl)piperidinium (4-AMP), and propanediammonium (PDA). These cations exhibit a structural characteristic distinct from RP perovskites^[64–66]. Each organic cation can integrate two adjacent inorganic layers in these DJ perovskites, effectively increasing adhesion and enabling interlayer charge transfer^[67–69]. Despite their enhanced structural stability compared to RP perovskites, DJ perovskites generally have lower permittivity, which increases the exciton binding energy and hinders charge separation. The small n -phase, referring to 2D perovskite phases with small n -values, can hinder charge transport due to strong quantum confinement effects, further exacerbating this problem^[70].

To optimize the performance of DJ THPSCs, researchers have focused on strategies that introduce various ammonium cations with different sizes and structures. This approach aims to control exciton binding energy and dielectric constant and suppress the formation of small n -phase, which hinders efficient charge transport^[71–73]. [Figure 4A](#) shows that (BEA)FA₂Sn₃I₁₀ film comprises perovskite quantum wells (QWs), which confine electrons and holes to a 2D plane. While these QWs are affected by the quantum confinement effect, the presence of BEA leads to a dominant $n = 2$ phase, effectively suppressing the formation of smaller n -phases. This can be observed in the transient absorption spectra (TA) in [Figure 4B](#), where the peak associated with the $n = 2$ phase shows a significant increase in intensity, indicating a reduced quantum confinement effect. This allows electrons and holes to move to a 3D-like perovskite environment, resulting in efficient charge separation and transfer^[74].

Yao *et al.* investigated the influence of phenylenediamine isomers on 2D THPSCs. They revealed that o-PDA, which has the largest dipole moment among the isomers, effectively reduced the exciton binding energy and improved charge dissociation and carrier transport^[75]. [Figure 4C](#) compares the dipole moment (μ) and dielectric constant (ϵ_r) of o-PDA, m-PDA, and p-PDA, demonstrating that o-PDA has the largest dipole moment and the highest dielectric constant among these isomers. This high ϵ_r facilitates exciton dissociation by lowering the energy required to separate bound electron-hole pairs. The strong hydrogen bond interaction between the o-PDA cation and the inorganic octahedron contributes to this larger ϵ_r in o-PDA films. Furthermore, o-PDA facilitated more efficient charge transfer between different n -phases within the perovskite structure. To further investigate the impact of amino substituent position on the dipole

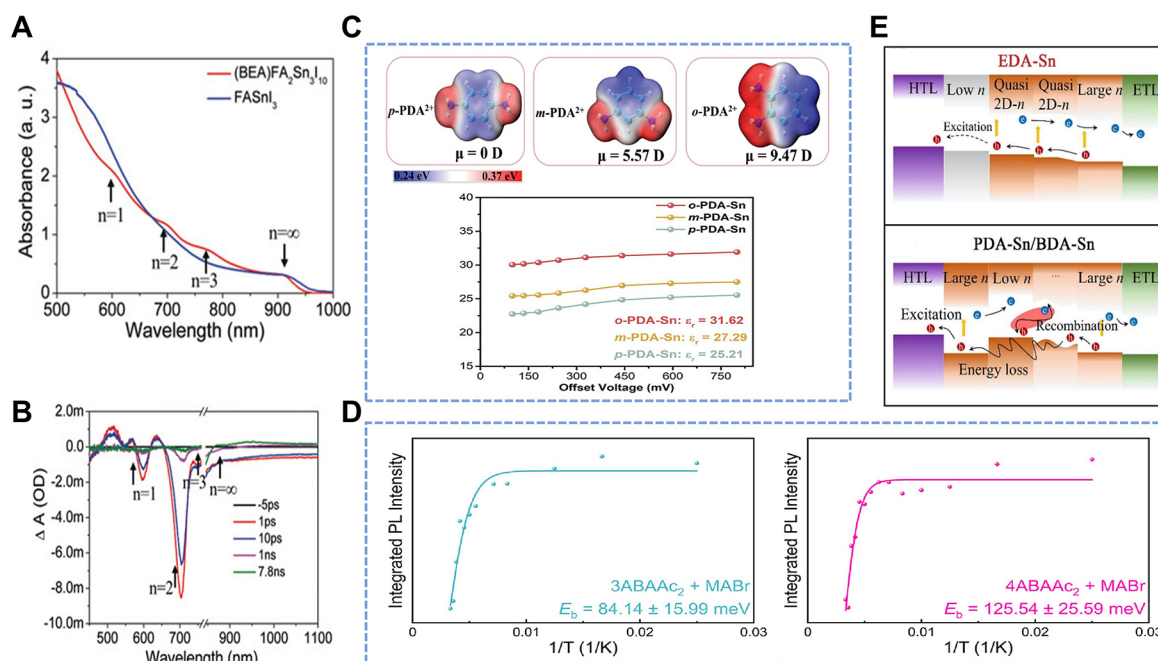


Figure 4. (A) UV-Vis absorption spectra of (BEA)FA₂Sn₃I₁₀ and FASnI₃ perovskite films; (B) TA spectra of (BEA)FA₂Sn₃I₁₀ film at various decay times: distinct bleach peaks at 610 nm ($n = 1$), 715 nm ($n = 2$), 780 nm ($n = 3$). This figure is quoted with permission from Li et al.^[74]; (C) Crystal structures, ESP diagrams, and calculated dipole moments of o-PDA-Sn, m-PDA-Sn, and p-PDA-Sn perovskites (top) and their relative dielectric constant as a function of offset voltage (bottom). This figure is quoted with permission from Yao et al.^[75]; (D) Integrated PL intensity and calculated E_b for 3ABAAc₂ + MABr (left) and 4ABAAc₂ + MABr (right) perovskite films. This figure is quoted with permission from Qian et al.^[76]; (E) Schematic band diagrams of carrier transport in EDA-Sn and PDA-Sn/BDA-Sn films. This figure is quoted with permission from Yao et al.^[77]. UV-Vis: ultraviolet-visible; PDA: propanediammonium; TA: transient absorption spectra; PL: photoluminescence.

moment, a study on 3ABAAc₂ and 4ABAAc₂ was conducted. The dipole moment was successfully increased by strategically positioning the amino substituent in 3ABAAc₂^[76]. This modification resulted in a significantly lower exciton binding energy (E_b) than 4ABAAc₂, as shown in Figure 4D, promoting exciton dissociation and charge transfer.

Further exploring the impact of organic spacers on perovskite film properties, researchers have investigated the effects of varying the spacer chain length^[77]. Specifically, they examined the effects of three different organic spacers with varying chain lengths on the properties of perovskite films: ethylenediammonium (EDA), PDA, and BDA. The shortest spacer, EDA, enhanced the film properties by reducing the proportion of the small n -phase, which hinders efficient charge transport. However, PDA-Sn and BDA-Sn films, which have longer spacer chain lengths, exhibited a higher proportion of these phases, hindering charge tunneling and transfer [Figure 4E]. These findings collectively demonstrate that optimizing the organic spacer is a promising strategy to improve the performance and stability of DJ THPSCs by controlling the exciton binding energy, dielectric constant, and phase distribution within the perovskite structure.

2D&3D mixed THPSCs

As previously mentioned, 3D perovskites offer high efficiency but are unstable and vulnerable to water and oxygen^[46,48]. On the other hand, 2D perovskites exhibit better stability, but their low charge mobility and wide bandgap limit light absorption^[78]. 2D&3D mixed (2D3D) perovskites, which combine 2D and 3D perovskites, offer the advantages of both increasing efficiency and stability^[55,79,80].

Similar to 2D perovskites, optimizing organic cations at the 2D3D interface is crucial in 2D3D perovskites^[81]. Interface engineering strengthens the bonding between 2D and 3D perovskites, enhances the protective effect of the 2D layer, and can even serve as a template to guide the crystal growth of 3D perovskites^[80,82-84]. However, if the optimization of the perovskite/2D material interface through precise control of the 2D material thickness and composition is not achieved, the deep-level traps can be formed, which may hinder the 3D layer growth and increase the energy barrier for charge transfer^[85]. The layer thickness of 2D RP perovskites can be effectively controlled by adjusting the precursor ratios of MACl and BA, enabling the synthesis of pure $n = 6$ and $n = 7$ structures^[86]. In addition, top-down synthetic methods, such as cosolvent evaporation and air solution interface crystallization, can precisely control the thickness and composition of 2D perovskite nanosheets by selecting spacer cations^[87]. Cresp *et al.* showed that thermal annealing can change the final n -value by inducing the loss of spacer cations in the RP structure and making the DJ phase more stable^[88]. Therefore, precise 2D3D interface control is essential to mitigate these problems by reducing interfacial recombination loss, increasing quasi-Fermi level splitting, and improving crystallization^[81,89].

As shown in Figure 5A, Wang *et al.* fabricated a 2D3D perovskite structure by incorporating guanidinium thiocyanate (GuaSCN)^[90]. This structure, which consists of a 3D FASnI₃ layer atop a 2D layer, exhibited improved open-circuit voltage (V_{oc}) due to increased quasi-Fermi level splitting, which led to better charge transport and reduced recombination. Organic spacers also play a crucial role in enhancing perovskite film crystallinity. For example, introducing PEASCN reduces the crystallization energy of the 2D perovskite structure, thus lowering the crystallization barrier and enabling rapid formation of the 2D structure^[91]. Figure 5B shows that PEASCN induces rapid 2D structure growth, covering the substrate and promoting perpendicular growth of the 2D/quasi-2D structure. This perpendicular growth results in highly aligned quasi-2D perovskite films by promoting the formation of a uniform crystal structure. Figure 5C shows that Grazing-incidence wide-angle X-ray scattering (GIWAXS) measurements of PEABr and PEABr-PEASCN films show that the PEABr film exhibits dispersed diffraction intensity and weaker orientation. In contrast, the PEABr-PEASCN film exhibits concentrated (100) plane diffraction intensity at 90°, indicating highly oriented growth.

Kang *et al.* compared PEA/DEA-based films, which exhibit only $n = 3$ and 3D phases, to PEA-based films with inhomogeneous 2D phases ($n = 2$ and $n = 3$)^[92]. The lower steric hindrance of DEA facilitated the formation of larger n -value phases, reduced lattice distortion and residual strain, and improved film quality. As shown in Figure 5D, the PEA-based film had an uneven surface potential and large tensile strain due to inhomogeneous low-dimensional phases. In contrast, the PEA/DEA-based film showed an improved surface morphology and reduced residual strain due to homogenized low-dimensional phases. Figure 5E further demonstrates the reduced tensile strain in the PEA/DEA-based film, as evidenced by the smaller slope of the linearly fitted $2\theta - \sin^2(\psi)$ function. These studies demonstrate that introducing organic spacers at the 2D3D interface can control crystal growth and improve strain management in 2D3D THPSCs, enhancing device performance and stability^[93]. To provide an overview of recent developments, Table 1 summarizes recent studies on 2D3D THPSCs, highlighting the perovskite composition, device structure, and achieved efficiency through strategic material incorporation.

ADDITIVES: BULK CRYSTAL OPTIMIZATION AND OXIDATION CONTROL

The easy oxidation of Sn²⁺ to Sn⁴⁺ and the resulting Sn vacancies are the leading causes of defects in THPSCs. This induces self-p-type carrier doping and consequently accelerates the nucleation and growth of perovskite crystals, negatively affecting device performance. Researchers have used various additives to optimize bulk crystal structure and control oxidation to mitigate these undesirable effects.

Table 1. Recent progress in 2D&3D mixed THPSCs.

Strategic material	Perovskite composition	PCE (%)	Stability/ PCE retained	Ref.
ANI (anilinium iodide)	$\text{AN}_2\text{FASnI}_3/\text{FA}_{0.8}\text{GA}_{0.2}\text{SnI}_3$	10.6	Air, unencapsulation 150 hr/ 100%	[94]
DFBAI (difluorobenzylammonium iodide)	$(\text{DFBA})_n\text{FA}_{1-n}\text{SnI}_3$	8.38	Air, unencapsulation 150 hr/ 100%	[95]
PEAI (phenylethylammonium iodide)	$\text{PEA}_2\text{FA}_4\text{Sn}_5\text{I}_{16}$	8.9	N_2 , unencapsulation 400 hr/ 80%	[96]
DEACI (diethylamine hydrochloride), HMCI (hydrazine monohydrochloride)	$\text{DEA}_2\text{FA}_8\text{Sn}_9\text{I}_{28-n}\text{Cl}_n$	9.47	N_2 , unencapsulation 14 day/ 90%	[97]
R-MBA (α -methylbenzylamine)	$(\text{R-MBA})_2\text{SnI}_4/\text{FASnI}_3$	10.73	N_2 , unencapsulation 120 day/ 90%	[98]
GuaSCN (guanidinium thiocyanate)	$\text{PEA}_2\text{FA}_1\text{Sn}_2\text{I}_7$	13.79	N_2 , 1200 hr/ 90%	[90]
TEAI (2-thiopheneethylammonium iodide)	$(\text{TEA})_2\text{MA}_{n-1}\text{Sn}_n\text{I}_{3n+1}$	6.8	-	[99]
CF_3PEAI [3-(trifluoromethyl) phenethylamine hydroiodide]	$(\text{CF}_3\text{PEA})_2\text{SnI}_4/\text{FAMASnI}_{2.75}\text{Br}_{0.25}$	10.35	N_2 , unencapsulation 1700 hr/ 80%	[100]
DFBAI (3,5-difluorobenzylammonium iodide)	$(\text{DFBA})_2\text{FASn}_2\text{I}_7/\text{FASnI}_3$	8.38	Air, unencapsulation 200 hr/ 100%	[95]
PEASCN (phenethylammonium thiocyanate)	$\text{FA}_{0.75}\text{MA}_{0.25}\text{SnI}_{2.75}\text{Br}_{0.25} : \text{PEASCN}$	12.88	N_2 , unencapsulation 2000 hr/ 80%	[101]
PEACI (phenethylammonium chloride)	$(\text{PEA})_2\text{Sn}_n\text{I}_{3n+1}/\text{FASnI}_3$	11.5	N_2 , unencapsulation 32 day/ 153%	[102]
GASCN (guanidine thiocyanate)	$\text{PEA}_{0.2}\text{FA}_{0.8}\text{SnI}_3/\text{GASCN}$	8.6	N_2 , unencapsulation 600 hr/ 88%	[103]
PEABr (phenylethylammonium bromide), PEASCN (phenethylammonium thiocyanate)	$\text{PEA}_2\text{FA}_{n-1}\text{Sn}_n\text{X}_{3n+1}$	14.6	N_2 , encapsulation 1000 hr/ 100%	[91]
PEABr (phenylethylammonium bromide)	$(\text{PEA})_2\text{SnI}_4/\text{FA}_{0.75}\text{MA}_{0.25}\text{SnI}_{2.75}\text{Br}_{0.25}$	11.94	N_2 , unencapsulation 2040 hr/ 94%	[104]
phDMADBr (1,4-phenyldimethylammonium dibromide diamine)	$\text{FASnI}_3 : \text{phDMADBr}$	11.44	N_2 , unencapsulation 1000 hr/ 90%	[105]
DFPDI (4,4-difluoropiperidinium iodide)	$\text{DFPD}_2\text{SnI}_4/\text{FASnI}_3$	13.34	N_2 , unencapsulation 1000 hr/ 90%	[106]
XS_2 (p-xylylenediammonium thiocyanate)	$\text{PEA}_{0.18}\text{XDA}_{0.01}\text{FA}_{0.8}\text{SnI}_{2.8}\text{SCN}_{0.2}$	14.31	N_2 , 25 day/ 95%	[107]
3AMPY (3-(aminomethyl)pyridine)	$\text{FASnI}_3 : 3\text{AMPYSnI}_4$	13.28	N_2 , unencapsulation 3000 hr/ 96%	[108]
FBEI (2,4-difluorobenzylammonium iodide)	$\text{FBE}_2\text{FA}_3\text{Sn}_4\text{I}_{13}$	9.25	Air, 24 hr/ 91%	[109]
EDAI ₂ (ethylenediammonium diiodide)	$(\text{EDA})\text{FA}_9\text{Sn}_{10}\text{I}_{31}$	7.07	Air, unencapsulation 200 hr/ 82%	[77]
MPI (morpholinium iodide)	$\text{MP}_2\text{SnI}_4/\text{FASnI}_3$	12.04	Air, unencapsulation 250 hr/ 77%	[110]
4-FPEAI (4-fluorophenethylammonium iodide)	$(4\text{-FPEA})_{0.1}\text{FA}_{0.9}\text{SnI}_3$	13.07	N_2 , unencapsulation 1200 hr/ 80%	[111]
DEACI (diethylammonium chloride)	$\text{PEA}_{0.125}\text{DEA}_{0.025}\text{FA}_{0.85}\text{SnI}_{2.85}\text{Br}_{0.125}\text{Cl}_{0.025}$	12.51	N_2 , unencapsulation 4600 hr/ 94%	[92]
D-HLH (D-homoserine lactone hydrochloride)	$\text{PEA}_{0.15}\text{FA}_{0.85}\text{SnI}_{2.85}\text{Br}_{0.15}$	12.45	N_2 , 70 day/ 85%	[112]
3-TEAI (2-(thiophen-3-yl)ethan-1-aminium iodide)	$(3\text{-TEA})_{0.2}\text{FA}_{0.8}\text{SnI}_3$	14.16	N_2 , unencapsulation 1960 hr/ 90%	[113]

PCE: power conversion efficiency; THPSC: tin halide perovskite solar cell.

Metal halides

Early research on THPSCs, developed as a replacement for LHPSCs, mainly focused on material optimization. Among the metal halide materials, SnF_2 , SnCl_2 , and SnBr_2 have been preferentially used to reduce the Sn vacancy concentration further and improve THPSC stability. Stabilizing THPSCs is critical for advancing lead-free PSCs^[114–116].

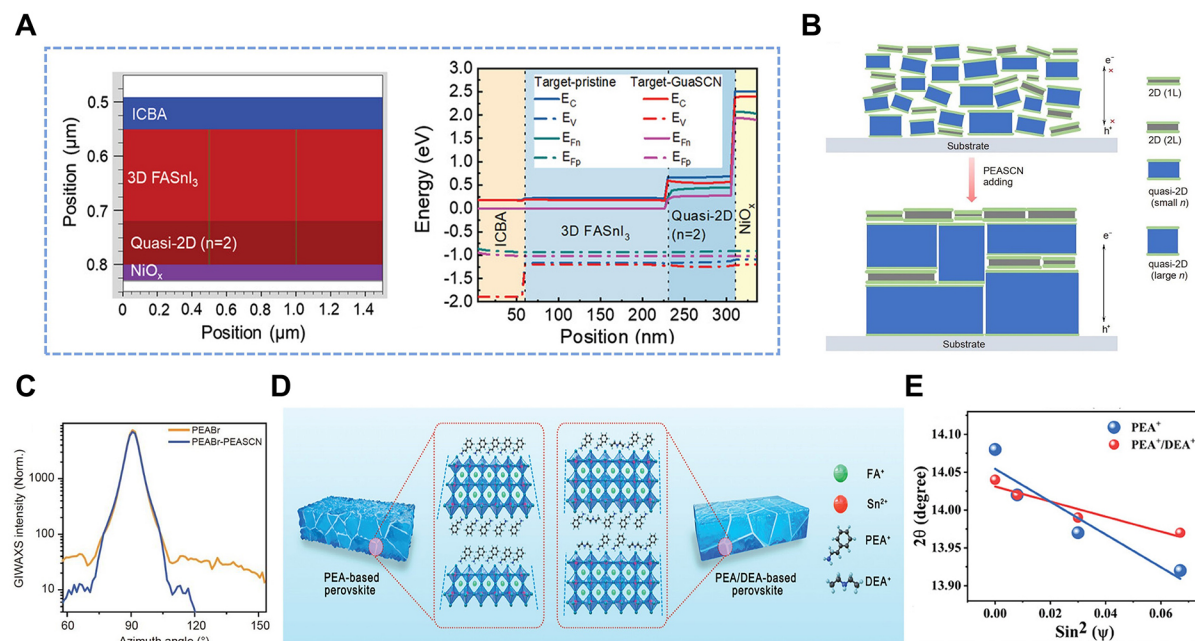


Figure 5. A: Device simulation results for the target-pristine or target-GuaSCN PSCs by the software Silvaco: Schematic PSC structure with vertical heterojunction used for simulation (left), and energy levels including the conduction band (E_c), the valence band (E_v), hole (E_{FP}), and electron (E_{FN}) quasi-Fermi levels across the whole devices under the open-circuit condition (right). This figure is quoted with permission from Wang *et al.*^[90]; B: Schematic of the crystallization mechanism of 2D/3D perovskite films with PEABr and PEABr-PEASCN; C: Azimuthally integrated GIWAXS intensity profiles at $q = 1 \text{ \AA}^{-1}$. This figure is quoted with permission from Li *et al.*^[91]; D: Schematic illustration of the impact of PEA-based and PEA/DEA-based films on surface morphology and strain in tin perovskite films; E: $2\theta - \sin^2(\psi)$ functions derived from grazing-incidence X-ray diffraction (GIXRD) results and their linear fits for PEA-based and PEA/DEA-based films. This figure is quoted with permission from Kang *et al.*^[92]. PSC: perovskite solar cell; PEA: phenethylammonium; DEA: diethylamine.

Various metal halides have been investigated as additives to improve the performance and stability of THPSCs. In Figure 6A, Heo *et al.* combined experimental investigations with first-principles density functional theory (DFT) calculations to uncover how SnX₂ additives influence THPSCs^[117]. Contrary to the conventional view that these additives primarily mitigate Sn vacancy defects (V_{Sn}), their findings reveal that they primarily contribute to surface passivation and stabilization of the THPSCs phase. SnBr₂ exhibits the highest adsorption energy among the additives, enabling superior phase stabilization and surface passivation. This results in an extended operational stability of approximately 100 hours and a power conversion efficiency of 4.3%. The addition of SnF₂ to FASnI₃ significantly increased the photocurrent density due to the increased hydrogen bonding, valence band alignment, and coverage of the perovskite layer^[118]. These studies suggest that SnF₂ can suppress Sn oxidation and improve the film morphology and coverage in inorganic and organic ammonium halide Sn perovskites.

Beyond SnX₂ additives, various other metal halides have been explored to enhance the performance and stability of THPSCs further. For example, as shown in Figure 6B, Liu *et al.* reported that incorporating a trace amount of InBr₂ effectively lifts the Fermi level and rearranges energy levels, improving interfacial band alignment while passivating defect states at the energy band tail^[119]. This results in enhanced charge transfer, reduced recombination losses, and optimized film morphology, crystallinity, and chemical uniformity. This minimizes defect densities and non-radiative recombination within the bulk perovskite. Furthermore, Ryu *et al.* introduced the rare earth element erbium chloride (ErCl₃) into THPSCs. ErCl₃ regulates nucleation and crystal growth, improving solution stability and optimizing film morphology

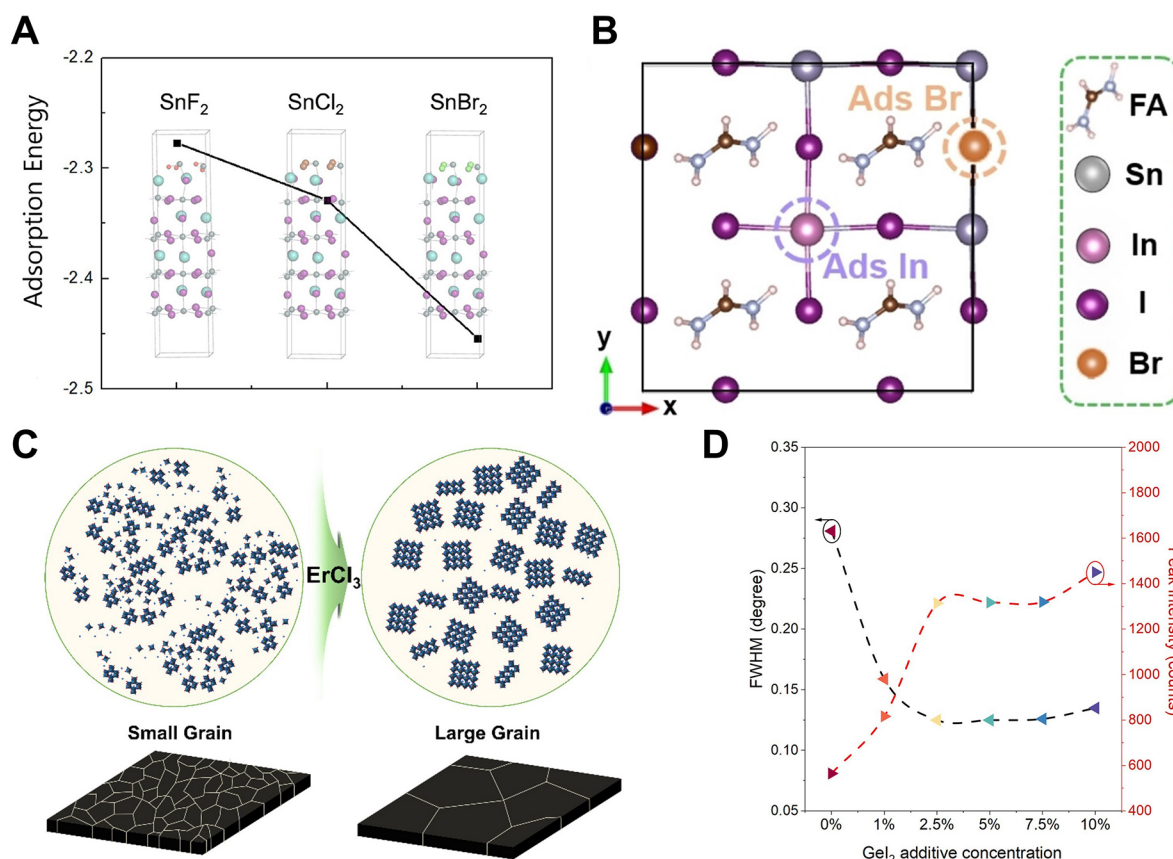


Figure 6. (A) Adsorption energies of SnBr₂, SnCl₂, and SnF₂ on the surface of CsSnI₃. This figure is quoted with permission from Heo et al. [121]; (B) DFT calculations of In and Br co-doped Sn perovskite (V_{Sn} and V_I represented the Sn and I vacancies). This figure is quoted with permission from Liu et al. [119]; (C) Schematic illustration of ErCl₃ incorporation effect on the precursor and film quality. This figure is quoted with permission from Ryu et al. [122]; (D) Summary of XRD intensity and FWHM of the (100) peak of THPSCs depend on the GeI₂ concentration. This figure is quoted with permission from Lai et al. [120]. DFT: density functional theory; THPSC: tin halide perovskite solar cell; XRD: X-ray diffraction; FWHM: full width half maximum.

[Figure 6C]. Figure 6D demonstrates that GeI₂, as an additive, regulates nucleation and crystallization in THPSCs [120]. In addition to ErCl₃, pyrazine and asparagine were simultaneously incorporated into the tin halide perovskite precursor solution to further improve the film quality and device performance. ErCl₃ regulates the nucleation and crystallization kinetics and inhibits Sn²⁺ oxidation, while pyrazine controls the crystallization rate and asparagine facilitates defect passivation and promotes grain growth. The combination of these additives leads to the overall device performance. Among metal halides, SnF₂ initially demonstrated the most significant enhancement in efficiency. Subsequently, GeI₂ was incorporated alongside SnF₂ [121–123]. Research indicated that an optimal GeI₂ concentration of 5% maximized efficiency. Exceeding this threshold leads to excessive lattice constant reduction, inducing lattice disorder and energy level misalignment, which can hinder charge transport and reduce device efficiency [124–126].

Using additional metal halides together with SnF₂ has recently improved stability and efficiency. However, metal halide additives alone cannot wholly address Sn oxidation in THPSCs despite effectively mitigating film oxidation. In addition to SnF₂, ammonium hypophosphite (AHP) has been reported to significantly enhance the energy level alignment between the FASnI₃ perovskite and Copper thiocyanate (CuSCN) hole transport layer, improving device performance [127]. Additionally, the Gallic Acid (GA) is reported to combine with SnCl₂ to give up the energy level of the conduction band of the perovskite film, thereby

improving the electron reduction^[128]. These results demonstrate that not only the SnF₂ additive but also other additives have broader effects, directly affecting the energy level alignment and electronic structure optimization in addition to the structural and chemical stabilization. Therefore, the introduction of diverse additives is crucial for these devices.

Lewis bases/acids

Among the metal halide additives used with perovskite precursors, SnF₂ can improve the photovoltaic performance of THPSCs by reducing charge traps caused by Sn vacancies and decreasing the charge carrier recombination rate. However, high concentrations of SnF₂ exceeding 10mol% can cause phase separation, resulting in pinholes and aggregations on the perovskite film^[129,130]. Phase separation can negatively affect the device's photovoltaic parameters; therefore, obtaining a uniform perovskite layer is essential.

Lewis base additives can effectively passivate Sn²⁺ defects and improve the performance of THPSCs^[131]. For example, Lee *et al.* used pyrazine to form a SnF₂-pyrazine complex that acts as a Lewis base additive, enhancing the film quality and performance of FASnI₃ perovskite films^[11]. Lewis acid additives can also enhance the performance of THPSCs by controlling the crystallization process and reducing non-radiative recombination. For instance, Li *et al.* adopted hypophosphorous acid (HPA) as an additive for CsSnI₃Br₂ perovskite films^[132]. This resulted in high-quality perovskite films with low Sn vacancies and stable phase.

Beyond these benefits, Lewis base/acid additives can also influence the crystallization process of perovskite. Introducing FAI into the A-site can significantly improve efficiency^[133-135]. However, the reaction between FAI and SnI₂ in the FASnI₃ perovskite precursor is fast due to the higher reactivity of SnI₂ as a Lewis acid^[136,137]. This fast reaction can lead to a trade-off between efficiency and stability when organic ammonium salts are incorporated into the perovskite composition^[138]. To mitigate this, employing Lewis base/acid additives with SnF₂ could control the crystallization rate and reduce the interaction strength between the precursor components^[71,139].

In addition to the Lewis base/acid additives mentioned above, Lewis neutral additives have also been investigated for their potential to improve the performance of THPSCs. For example, Deng *et al.* used polymethylmethacrylate (PMMA) as a compatible additive for FASnI₃ precursor solutions and achieved a power conversion efficiency of 3.62%^[140]. However, Lewis neutral additives were only partially compatible due to their limited ability to control the crystallization process.

Jokar *et al.* demonstrated the effectiveness of ethylenediammonium diiodide (EDAI₂) in improving stability and performance^[71]. EDAI₂ also acted as a dopant and reducing agent to suppress Sn oxidation^[141]. Similarly, n-propylammonium iodide (PAI) facilitated the template growth of FASnI₃ crystals, resulting in a highly crystalline film with improved performance and stability^[142,143]. Moreover, Song's group introduced pyrazine and asparagine to control the crystallization rate^[144,145]. In addition, pseudohalogens of the thiocyanate (SCN⁻) series form Sn-donor complexes in tin perovskites^[90,146-149]. Combining these additives forms a stable intermediate phase, improving device efficiency. Table 2 summarizes recent studies on additives in THPSCs, including the perovskite composition, device structure, and achieved efficiency.

As presented in Tables 1 and 2, both 2D materials and additives play a crucial role in optimizing the efficiency and stability of THPSCs. While 2D materials primarily enhance charge transport properties, passivate interfacial defects, and improve environmental stability, additives address key structural challenges by suppressing Sn²⁺ oxidation and regulating crystallization.

Table 2. PV parameters of the reported inverted THPSCs with various additives

Perovskite composition	Additives	J_{sc} (mA/cm ²)	V_{oc} (V)	FF (%)	PCE(%)	Publication Year	Ref.
CsSnI ₃	SnF ₂	10.21	0.52	62.5	3.31	2016	[129]
CsSnI ₂ Br	SnF ₂ + HPA (hypophosphorous acid)	17.4	0.31	57	3.2	2016	[132]
FASnI ₃	SnF ₂	22.07	0.465	60.67	6.22	2016	[135]
FA _{0.75} MA _{0.25} SnI ₃	SnF ₂	21.2	0.61	62.7	8.12	2017	[150]
PEAFASnI ₃	SnF ₂	24.1	0.525	71	9.0	2017	[151]
PEA _{0.15} FA _{0.85} SnI ₃	SnF ₂ + NH ₄ SCN (ammonium thiocyanate)	22.0	0.61	70.1	9.41	2018	[147]
GA _{0.2} FA _{0.8} SnI ₃	SnF ₂ + EDAl ₂	21.2	0.619	72.9	9.6	2018	[152]
FASnI ₃	SnF ₂ + PPAl (phenyl-2-propen-1-ammonium iodide)	23.34	0.56	73.5	9.61	2019	[153]
FA _{0.98} EDA _{0.01} SnI ₃	SnF ₂ + DAE (1,2-diaminoethane)	22.8	0.56	74	10.18	2019	[154]
FASnI ₃	SnF ₂ + LFA (liquid formic acid)	22.25	0.628	74.2	10.37	2020	[155]
Cs _{0.2} FA _{0.8} SnI ₃	SnF ₂ + SnCl ₂ + EDAl ₂	21.6	0.64	75.2	10.4	2020	[121]
FASnI ₃	SnF ₂ + FOEI (pentafluorophen-oxyethylammonium iodide)	21.59	0.67	75	10.81	2020	[156]
FASnI ₃	4AMPI ₂ [4-(aminomethyl)piperidinium diiodide]	21.15	0.69	74	10.86	2020	[157]
FASnI ₃	SnF ₂ + PHCl (phenylhydrazine hydrochloride)	23.5	0.76	64	11.4	2020	[158]
FA _{0.75} MA _{0.25} SnI ₃	SnF ₂ + TM-DHP [1,4-bis(trimethylsilyl)-2,3,5,6-tetramethyl-1,4-dihydropyrazine]	22.0	0.76	69.0	11.5	2020	[159]
FASnI ₃	SnF ₂ + PAI (n-propylammonium iodide)	22.37	0.73	72	11.78	2020	[143]
PEA _{0.15} FA _{0.85} SnI ₃	SnF ₂ + NH ₄ SCN	17.4	0.94	75	12.4	2020	[160]
FASnI _{2.875} Br _{0.125}	SnF ₂ + SnBr ₂ + PHCl	23.02	0.81	72	13.4	2021	[114]
FA _{0.75} MA _{0.25} SnI _{2.75} Br _{0.25}	SnF ₂ + PEAI + 4A3HA (4-amino-3-hydroxybenzoic acid)	21.02	0.9	71.22	13.43	2022	[161]
FASnI ₃	SnF ₂ + EDADI + MHATFA (6-maleimido-hexanehydrazide trifluoroacetate)	23.27	0.803	72.99	13.64	2022	[162]
PEA _{0.15} FA _{0.85} SnI _{2.85} Br _{0.15}	SnF ₂ + NH ₄ SCN + GAA (2-Guanidinoacetic acid)	19.66	0.94	74.9	13.7	2022	[148]
PEA ₂ FA ₁ Sn ₂ I ₇	SnF ₂ + GuaSCN	20.32	1.01	67.2	13.79	2022	[90]
FASnI ₃	SnF ₂ + EDAl ₂ + theophylline-Br (8-bromotheophylline)	24.2	0.75	76	13.8	2022	[163]
FA _{0.98} EDA _{0.01} SnI ₃	SnI ₂ + Gel ₂ + FBZAI (4-fluorobenzylammonium iodide)	22.87	0.778	77.81	13.85	2022	[164]
PEA _{0.15} FA _{0.85} SnI ₃	Trimethylthiourea	21.02	0.9	71.22	14.3	2022	[165]
FASnI ₃	SnF ₂ + POEBr (2-phenoxyethylamine bromide)	22.44	0.855	74.7	14.32	2023	[166]
FASnI ₃	SnI ₂ + Gel ₂ + BrDS (2,8-dibromo-dibenzothiophene-S,S-dioxide)	23.86	0.79	79.45	14.98	2024	[167]
FASnI ₃	SnF ₂ + NH ₄ SCN + TEASCN + NH ₅ F ₂ (2-thiopheneethylamine thiocyanate)	20.12	0.97	76.61	15.04	2024	[149]

PCE: power conversion efficiency; THPSC: tin halide perovskite solar cell; PV: photovoltaics.

Although 2D materials contribute significantly to devices' electronic properties and robustness, their role in mitigating bulk defects and maintaining long-term stability is limited. In contrast, additives provide a complementary approach that directly affects the lifetime and operating efficiency of devices by stabilizing the perovskite phase, reducing the trap state density, and optimizing film morphology. Therefore, 2D materials and additives are essential to achieve high-performance and durable THPSCs. A dual approach that strategically integrates the two components is essential to achieve multifaceted optimization, thereby improving charge carrier dynamics and enhancing structural stability.

FUTURE RESEARCH PROSPECTS FOR THPSCS

This review explores the use of 2D materials and additive engineering in THPSCs, particularly those based on Sn. These devices have enabled significant advancements in this field. However, the stability of THPSCs, particularly their air stability, remains a significant challenge due to Sn^{2+} oxidation and subsequent decomposition of perovskite upon exposure to oxygen and water. Therefore, future research should focus on utilizing both 2D materials and additives to enhance the performance and stability of THPSCs.

Previous studies have demonstrated that 2D materials can improve charge transport and moisture resistance, but their effectiveness in fully passivating grain boundary defects and controlling deep trap states is still limited. Further research should prioritize developing novel 2D materials and additives with tailored functionalities to address the challenges of Sn^{2+} oxidation and energy level alignment in THPSCs. Long-term stability evaluations of THPSCs incorporating these combined strategies under diverse environmental conditions are also crucial.

In particular, precision engineering of the 2D/3D interface can enhance device performance by optimizing charge extraction and minimizing recombination losses. Furthermore, while additives effectively suppress oxidation and passivate defects, their influence on perovskite crystallization kinetics requires further investigation to improve film uniformity and reduce non-radiative recombination. Moving forward in this direction will contribute significantly to developing high-performance THPSCs.

CONCLUSIONS

This review paper presents an in-depth analysis of defect control, performance improvement, and stability assurance, which are key tasks for commercializing THPSCs, attracting attention as next-generation solar cell technology. In particular, we focus on eco-friendly THPSCs that can solve toxicity problems while maintaining the excellent optoelectronic properties of LHPSCs and intensively discuss strategies for utilizing 2D materials and additives to solve the problems of Sn^{2+} to Sn^{4+} oxidation, defect generation, and device performance degradation caused by the unique properties of tin-based perovskite materials.

2D materials have excellent electrical properties, high surface area, and flexible structural features, which contribute to improving the charge transport ability of THPSCs, effectively passivating defects, and enhancing moisture stability. In addition, we confirmed that the bulk crystal optimization and oxidation control of THPSCs can be achieved through various additives to improve performance.

This review paper emphasizes that the performance of THPSC can be maximized through the synergistic effects of 2D materials and additives. 2D materials play a role in improving the interface properties and enhancing moisture stability, and additives play a role in optimizing the bulk crystal structure and controlling oxidation. By appropriately utilizing 2D materials and additives, the efficiency and stability of THPSC can be simultaneously improved, significantly increasing the possibility of commercialization.

Future research should focus on maximizing the synergistic effects of 2D materials and additives, developing new 2D materials and additives, interface engineering, and evaluating long-term stability. These efforts are expected to lead to the development of high-efficiency, high-stability THPSCs and accelerate their commercialization.

DECLARATIONS

Authors' contributions

Made substantial contributions to the conception and design of the study: Kim, J. H.; D. H. Ryu, D. H.; Song, C. E.

Performed data analysis and interpretation: Jeong, J.

Conducted data interpretation: Im, S. H.

Financial support and sponsorship

This work was supported by the National Research Foundation (NRF) (NRF-RS-2021-NR059606), the National Research Council of Science and Technology (Grant No. Global-23-007), and the Korea Research Institute of Chemical Technology (KRICT) (No. KS2422-10) of the Republic of Korea.

Availability of data and materials

Not applicable.

Conflicts of interest

S. H. Im is the Guest Editor of the Special Issue of “Research on the Microstructure and Performance of Perovskite Materials”, but he is not involved in any steps of editorial processing, notably including reviewer selection, manuscript handling, and decision making. The other authors declared that there are no conflicts of interest.

Ethical approval and consent to participate

Not applicable.

Consent for publication

Not applicable.

Copyright

© The Author(s) 2025.

REFERENCES

1. Chen, Q.; De, M. N.; Yang, Y.; et al. Under the spotlight: the organic-inorganic hybrid halide perovskite for optoelectronic applications. *Nano. Today*. **2015**, *10*, 355-96. DOI
2. Manser, J. S.; Christians, J. A.; Kamat, P. V. Intriguing optoelectronic properties of metal halide perovskites. *Chem. Rev.* **2016**, *116*, 12956-3008. DOI PubMed
3. Zhao, X.; Yang, D.; Ren, J.; Sun, Y.; Xiao, Z.; Zhang, L. Rational design of halide double perovskites for optoelectronic applications. *Joule* **2018**, *2*, 1662-73. DOI
4. NREL Best Research-Cell Efficiency Chart. Available from: <https://www.nrel.gov/pv/cell-efficiency.html> [Last accessed 18 Apr 2025].
5. Binek, A.; Petrus, M. L.; Huber, N.; et al. Recycling perovskite solar cells to avoid lead waste. *ACS. Appl. Mater. Interfaces*. **2016**, *8*, 12881-6. DOI
6. Jiang, Y.; Qiu, L.; Juarez-perez, E. J.; et al. Reduction of lead leakage from damaged lead halide perovskite solar modules using self-healing polymer-based encapsulation. *Nat. Energy*. **2019**, *4*, 585-93. DOI
7. Li, J.; Cao, H. L.; Jiao, W. B.; et al. Biological impact of lead from halide perovskites reveals the risk of introducing a safe threshold. *Nat. Commun.* **2020**, *11*, 310. DOI PubMed PMC
8. Bai, F.; Hu, Y.; Hu, Y.; Qiu, T.; Miao, X.; Zhang, S. Lead-free, air-stable ultrathin Cs₃Bi₂I₉ perovskite nanosheets for solar cells. *Solar. Energy. Materials. and. Solar. Cells*. **2018**, *184*, 15-21. DOI
9. Turkevych, I.; Kazaoui, S.; Ito, E.; et al. Photovoltaic rudorffites: lead-free silver bismuth halides alternative to hybrid lead halide perovskites. *ChemSusChem* **2017**, *10*, 3754-9. DOI
10. Krishnamoorthy, T.; Ding, H.; Yan, C.; et al. Lead-free germanium iodide perovskite materials for photovoltaic applications. *J. Mater. Chem. A*. **2015**, *3*, 23829-32. DOI
11. Lee, S. J.; Shin, S. S.; Kim, Y. C.; et al. Fabrication of efficient formamidinium tin iodide perovskite solar cells through SnF₂-

- pyrazine complex. *J. Am. Chem. Soc.* **2016**, *138*, 3974-7. DOI
12. Nishimura, K.; Kamarudin, M. A.; Hirofani, D.; et al. Lead-free tin-halide perovskite solar cells with 13% efficiency. *Nano. Energy.* **2020**, *74*, 104858. DOI
 13. Toshniwal, A.; Kheraj, V. Development of organic-inorganic tin halide perovskites: a review. *Solar. Energy.* **2017**, *149*, 54-9. DOI
 14. Giustino, F.; Snaith, H. J. Toward lead-free perovskite solar cells. *ACS. Energy. Lett.* **2016**, *1*, 1233-40. DOI
 15. Yaffe, O.; Chernikov, A.; Norman, Z. M.; et al. Excitons in ultrathin organic-inorganic perovskite crystals. *Phys. Rev. B.* **2015**, *92*. DOI
 16. Herz, L. M. Charge-carrier mobilities in metal halide perovskites: fundamental mechanisms and limits. *ACS. Energy. Lett.* **2017**, *2*, 1539-48. DOI
 17. Monahan, D. M.; Guo, L.; Lin, J.; Dou, L.; Yang, P.; Fleming, G. R. Room-temperature coherent optical phonon in 2D electronic spectra of $\text{CH}_3\text{NH}_3\text{PbI}_3$ perovskite as a possible cooling bottleneck. *J. Phys. Chem. Lett.* **2017**, *8*, 3211-5. DOI
 18. Baranowski, M.; Plochocka, P. Excitons in metal-halide perovskites. *Adv. Energy. Mater.* **2020**, *10*, 1903659. DOI
 19. Fatema, K.; Arefin, M. S. Enhancing the efficiency of Pb-based and Sn-based perovskite solar cell by applying different ETL and HTL using SCAPS-ID. *Opt. Mater.* **2022**, *125*, 112036. DOI
 20. Guo, R.; Rao, L.; Liu, Q.; et al. Atmospheric stable and flexible Sn-based perovskite solar cells via a bio-inspired antioxidative crystal template. *J. Energy. Chem.* **2022**, *66*, 612-8. DOI
 21. Shi, T.; Zhang, H.; Meng, W.; et al. Effects of organic cations on the defect physics of tin halide perovskites. *J. Mater. Chem. A.* **2017**, *5*, 15124-9. DOI
 22. Zhu, C.; Niu, X.; Fu, Y.; et al. Strain engineering in perovskite solar cells and its impacts on carrier dynamics. *Nat. Commun.* **2019**, *10*, 815. DOI PubMed PMC
 23. Awais, M.; Kirsch, R. L.; Yeddu, V.; Saidaminov, M. I. Tin halide perovskites going forward: frost diagrams offer hints. *ACS. Materials. Lett.* **2021**, *3*, 299-307. DOI
 24. Zhou, Y.; Saliba, M. Zooming In on metal halide perovskites: new energy frontiers emerge. *ACS. Energy. Lett.* **2021**, *6*, 2750-4. DOI
 25. Zhang, C.; Park, N. Materials and methods for cost-effective fabrication of perovskite photovoltaic devices. *Commun. Mater.* **2024**, *5*, 636. DOI
 26. Scalón, L.; Nogueira, C. A.; Fonseca, A. F. V.; et al. 2D phase formation on 3D perovskite: insights from molecular stiffness. *ACS. Appl. Mater. Interfaces.* **2024**, *16*, 51727-37. DOI PubMed PMC
 27. Wu, S.; Chen, Z.; Yip, H.; Jen, A. K. The evolution and future of metal halide perovskite-based optoelectronic devices. *Matter* **2021**, *4*, 3814-34. DOI
 28. Teo, S. H.; Ng, C. H.; Ng, Y. H.; Islam, A.; Hayase, S.; Taufiq-yap, Y. H. Resolve deep-rooted challenges of halide perovskite for sustainable energy development and environmental remediation. *Nano. Energy.* **2022**, *99*, 107401. DOI
 29. Kojima, A.; Teshima, K.; Shirai, Y.; Miyasaka, T. Organometal halide perovskites as visible-light sensitizers for photovoltaic cells. *J. Am. Chem. Soc.* **2009**, *131*, 6050-1. DOI
 30. Kim, H. S.; Lee, C. R.; Im, J. H.; et al. Lead iodide perovskite sensitized all-solid-state submicron thin film mesoscopic solar cell with efficiency exceeding 9%. *Sci. Rep.* **2012**, *2*, 591. DOI PubMed PMC
 31. Park, N. Organometal perovskite light absorbers toward a 20% efficiency low-cost solid-state mesoscopic solar cell. *J. Phys. Chem. Lett.* **2013**, *4*, 2423-9. DOI
 32. Wang, K.; Jin, Z.; Liang, L.; et al. All-inorganic cesium lead iodide perovskite solar cells with stabilized efficiency beyond 15. *Nat. Commun.* **2018**, *9*, 4544. DOI PubMed PMC
 33. Glazer, A. M. The classification of tilted octahedra in perovskites. *Acta. Crystallogr. B. Struct. Crystallogr. Cryst. Chem.* **1972**, *28*, 3384-92. DOI
 34. Pellet, N.; Gao, P.; Gregori, G.; et al. Mixed-organic-cation perovskite photovoltaics for enhanced solar-light harvesting. *Angew. Chem. Int. Ed. Engl.* **2014**, *53*, 3151-7. DOI
 35. Wang, Y.; Lin, J.; He, Y.; et al. Improvement in the performance of inverted 3D/2D perovskite solar cells by ambient exposure. *Solar. RRL.* **2022**, *6*, 2200224. DOI
 36. Wu, G.; Yang, T.; Li, X.; et al. Molecular engineering for two-dimensional perovskites with photovoltaic efficiency exceeding 18%. *Matter* **2021**, *4*, 582-99. DOI
 37. El-Ballouli, A. O.; Bakr, O. M.; Mohammed, O. F. Structurally tunable two-dimensional layered perovskites: from confinement and enhanced charge transport to prolonged hot carrier cooling dynamics. *J. Phys. Chem. Lett.* **2020**, *11*, 5705-18. DOI PubMed PMC
 38. Yi, C.; Luo, J.; Meloni, S.; et al. Entropic stabilization of mixed A-cation ABX_3 metal halide perovskites for high performance perovskite solar cells. *Energy. Environ. Sci.* **2016**, *9*, 656-62. DOI
 39. Huang, J.; Tan, S.; Lund, P. D.; Zhou, H. Impact of H_2O on organic-inorganic hybrid perovskite solar cells. *Energy. Environ. Sci.* **2017**, *10*, 2284-311. DOI
 40. Lin, Y.; Chen, B.; Fang, Y.; et al. Excess charge-carrier induced instability of hybrid perovskites. *Nat. Commun.* **2018**, *9*, 4981. DOI PubMed PMC
 41. Luo, S.; Daoud, W. A. Recent progress in organic-inorganic halide perovskite solar cells: mechanisms and material design. *J. Mater. Chem. A.* **2015**, *3*, 8992-9010. DOI
 42. Khatoon, S.; Kumar, Y. S.; Chakravorty, V.; et al. Perovskite solar cell's efficiency, stability and scalability: a review. *Mater. Sci. Energy. Technol.* **2023**, *6*, 437-59. DOI

43. Kore, B. P.; Jamshidi, M.; Gardner, J. M. The impact of moisture on the stability and degradation of perovskites in solar cells. *Mater. Adv.* **2024**, *5*, 2200-17. DOI
44. Pitaro, M.; Tekelenburg, E. K.; Shao, S.; Loi, M. A. Tin halide perovskites: from fundamental properties to solar cells. *Adv. Mater.* **2022**, *34*, e2105844. DOI PubMed PMC
45. Ruddlesden, S. N.; Popper, P. New compounds of the K_2NiF_4 type. *Acta. Cryst.* **1957**, *10*, 538-9. DOI
46. Smith, I. C.; Hoke, E. T.; Solis-Ibarra, D.; McGehee, M. D.; Karunadasa, H. I. A layered hybrid perovskite solar-cell absorber with enhanced moisture stability. *Angew. Chem. Int. Ed. Engl.* **2014**, *53*, 11232-5. DOI PubMed
47. Stoumpos, C. C.; Cao, D. H.; Clark, D. J.; et al. Ruddlesden-Popper hybrid lead iodide perovskite 2D homologous semiconductors. *Chem. Mater.* **2016**, *28*, 2852-67. DOI
48. Chen, Y.; Sun, Y.; Peng, J.; et al. Tailoring organic cation of 2D air-stable organometal halide perovskites for highly efficient planar solar cells. *Advanced. Energy. Materials.* **2017**, *7*, 1700162. DOI
49. Cheng, P.; Xu, Z.; Li, J.; et al. Highly efficient Ruddlesden-Popper halide perovskite $PA_2MA_4Pb_5I_{16}$ Solar Cells. *ACS. Energy. Lett.* **2018**, *3*, 1975-82. DOI
50. Hong, X.; Ishihara, T.; Nurmikko, A. V. Dielectric confinement effect on excitons in PbI_4 -based layered semiconductors. *Phys. Rev. B. Condens. Matter.* **1992**, *45*, 6961-4. DOI PubMed
51. Guo, Z.; Wu, X.; Zhu, T.; Zhu, X.; Huang, L. Electron-phonon scattering in atomically thin 2D perovskites. *ACS. Nano.* **2016**, *10*, 9992-8. DOI
52. Gélvez-Rueda, M. C.; Hutter, E. M.; Cao, D. H.; et al. Interconversion between free charges and bound excitons in 2D hybrid lead halide perovskites. *J. Phys. Chem. C. Nanomater. Interfaces.* **2017**, *121*, 26566-74. DOI PubMed PMC
53. Fu, W.; Wang, J.; Zuo, L.; et al. Two-dimensional perovskite solar cells with 14.1% power conversion efficiency and 0.68% external radiative efficiency. *ACS. Energy. Lett.* **2018**, *3*, 2086-93. DOI
54. Lai, H.; Kan, B.; Liu, T.; et al. Two-dimensional Ruddlesden-Popper perovskite with nanorod-like morphology for solar cells with efficiency exceeding 15%. *J. Am. Chem. Soc.* **2018**, *140*, 11639-46. DOI
55. Shao, M.; Bie, T.; Yang, L.; et al. Over 21% efficiency stable 2D perovskite solar cells. *Adv. Mater.* **2022**, *34*, e2107211. DOI
56. Kayesh, M. E.; Matsuishi, K.; Kaneko, R.; et al. Coadditive engineering with 5-ammonium valeric acid iodide for efficient and stable Sn perovskite solar cells. *ACS. Energy. Lett.* **2019**, *4*, 278-84. DOI
57. Ma, L.; Ju, M. G.; Dai, J.; Zeng, X. C. Tin and germanium based two-dimensional Ruddlesden-Popper hybrid perovskites for potential lead-free photovoltaic and photoelectronic applications. *Nanoscale* **2018**, *10*, 11314-9. DOI PubMed
58. Wang, D.; Liang, P.; Dong, Y.; Shu, H.; Liu, Z. Electronic and optical properties of layered Ruddlesden Popper hybrid $X_2(MA)_{n-1}SnI_{3n+1}$ perovskite insight by first principles. *J. Phys. Chem. Solids.* **2020**, *144*, 109510. DOI
59. Cao, D. H.; Stoumpos, C. C.; Yokoyama, T.; et al. Thin films and solar cells based on semiconducting two-dimensional Ruddlesden-Popper $(CH_3(CH_2)_3NH_3)_2(CH_3NH_3)_{n-1}SnI_{3n+1}$ perovskites. *ACS. Energy. Lett.* **2017**, *2*, 982-90. DOI
60. Dion, M.; Ganne, M.; Tournoux, M. Nouvelles familles de phases $M^{II}M_2Nb_3O_{10}$ a feuillets "perovskites". *Mater. Res. Bull.* **1981**, *16*, 1429-35. DOI
61. Jacobson, A. J.; Johnson, J. W.; Lewandowski, J. T. Interlayer chemistry between thick transition-metal oxide layers: synthesis and intercalation reactions of $K[Ca_2Na_{n-3}Nb_nO_{3n+1}]$ (3 .ltoreq. n .ltoreq. 7). *Inorg. Chem.* **1985**, *24*, 3727-9. DOI
62. Ahmad, S.; Fu, P.; Yu, S.; et al. Dion-Jacobson phase 2D layered perovskites for solar cells with ultrahigh stability. *Joule* **2019**, *3*, 794-806. DOI
63. Gong, J.; Hao, M.; Zhang, Y.; Liu, M.; Zhou, Y. Layered 2D halide perovskites beyond the Ruddlesden-Popper phase: tailored interlayer chemistries for high-performance solar cells. *Angew. Chem. Int. Ed. Engl.* **2022**, *61*, e202112022. DOI
64. Safdari, M.; Svensson, P. H.; Hoang, M. T.; Oh, I.; Kloo, L.; Gardner, J. M. Layered 2D alkyldiammonium lead iodide perovskites: synthesis, characterization, and use in solar cells. *J. Mater. Chem. A.* **2016**, *4*, 15638-46. DOI
65. Mao, L.; Ke, W.; Pedesseau, L.; et al. Hybrid Dion-Jacobson 2D lead iodide perovskites. *J. Am. Chem. Soc.* **2018**, *140*, 3775-83. DOI
66. Ma, C.; Shen, D.; Ng, T. W.; Lo, M. F.; Lee, C. S. 2D Perovskites with short interlayer distance for high-performance solar cell application. *Adv. Mater.* **2018**, *30*, e1800710. DOI PubMed
67. Boeijs, Y.; Van, G. W. T. M.; Zhang, Y.; et al. Tailoring interlayer charge transfer dynamics in 2D perovskites with electroactive spacer molecules. *J. Am. Chem. Soc.* **2023**, *145*, 21330-43. DOI
68. Li, X.; Ke, W.; Traoré, B.; et al. Two-dimensional Dion-Jacobson hybrid lead iodide perovskites with aromatic diammonium cations. *J. Am. Chem. Soc.* **2019**, *141*, 12880-90. DOI
69. Lin, Y. L.; Johnson, J. C. Interlayer triplet energy transfer in dion-jacobson two-dimensional lead halide perovskites containing naphthalene diammonium cations. *J. Phys. Chem. Lett.* **2021**, *12*, 4793-8. DOI
70. Ghosh, D.; Acharya, D.; Pedesseau, L.; et al. Charge carrier dynamics in two-dimensional hybrid perovskites: Dion-Jacobson vs. Ruddlesden-Popper phases. *J. Mater. Chem. A.* **2020**, *8*, 22009-22. DOI
71. Jokar, E.; Chien, C.; Fathi, A.; Rameez, M.; Chang, Y.; Diao, E. W. Slow surface passivation and crystal relaxation with additives to improve device performance and durability for tin-based perovskite solar cells. *Energy. Environ. Sci.* **2018**, *11*, 2353-62. DOI
72. Ke, W.; Stoumpos, C. C.; Spanopoulos, I.; Chen, M.; Wasielewski, M. R.; Kanatzidis, M. G. Diammonium cations in the $FASnI_3$ perovskite structure lead to lower dark currents and more efficient solar cells. *ACS. Energy. Lett.* **2018**, *3*, 1470-6. DOI
73. Chen, M.; Ju, M.; Hu, M.; et al. Lead-Free Dion-Jacobson Tin Halide Perovskites for Photovoltaics. *ACS. Energy. Lett.* **2019**, *4*, 276-

7. DOI

74. Li, P.; Liu, X.; Zhang, Y.; et al. Low-dimensional Dion-Jacobson-phase lead-free perovskites for high-performance photovoltaics with improved stability. *Angew. Chem. Int. Ed. Engl.* **2020**, *59*, 6909-14. DOI
75. Yao, H.; Wu, T.; Wu, C.; Ding, L.; Hua, Y.; Hao, F. Structural tailoring the phenylenediamine isomers to obtain 2D Dion-Jacobson tin perovskite solar cells with record efficiency. *Adv. Funct. Mater.* **2024**, *34*, 2312287. DOI
76. Qian, J.; Li, Y.; Shen, Y.; et al. Dion-Jacobson-phase 2D Sn-based perovskite comprising a high dipole moment of π -conjugated short-chain organic spacers for high-performance solar cell applications. *ACS. Nano.* **2024**, *18*, 15055-66. DOI
77. Yao, H.; Shi, C.; Wu, T.; et al. Regulation of the quantum barrier and carrier transport toward high-efficiency quasi-2D Dion-Jacobson tin perovskite solar cells. *J. Energy. Chem.* **2024**, *95*, 200-7. DOI
78. Cao, D. H.; Stoumpos, C. C.; Farha, O. K.; Hupp, J. T.; Kanatzidis, M. G. 2D homologous perovskites as light-absorbing materials for solar cell applications. *J. Am. Chem. Soc.* **2015**, *137*, 7843-50. DOI PubMed
79. Quan, L. N.; Yuan, M.; Comin, R.; et al. Ligand-stabilized reduced-dimensionality perovskites. *J. Am. Chem. Soc.* **2016**, *138*, 2649-55. DOI
80. Teale, S.; Proppe, A. H.; Jung, E. H.; et al. Dimensional mixing increases the efficiency of 2D/3D perovskite solar cells. *J. Phys. Chem. Lett.* **2020**, *11*, 5115-9. DOI
81. Krishna, A.; Gottis, S.; Nazeeruddin, M. K.; Sauvage, F. Mixed dimensional 2D/3D Hybrid perovskite absorbers: the future of perovskite solar cells? *Adv. Funct. Mater.* **2019**, *29*, 1806482. DOI
82. Li, H.; Zhang, C.; Gong, C.; et al. 2D/3D heterojunction engineering at the buried interface towards high-performance inverted methylammonium-free perovskite solar cells. *Nat. Energy.* **2023**, *8*, 946-55. DOI
83. Wang, J.; Luo, S.; Lin, Y.; et al. Templated growth of oriented layered hybrid perovskites on 3D-like perovskites. *Nat. Commun.* **2020**, *11*, 582. DOI PubMed PMC
84. Zhou, T.; Xu, Z.; Wang, R.; Dong, X.; Fu, Q.; Liu, Y. Crystal growth regulation of 2D/3D perovskite films for solar cells with both high efficiency and stability. *Adv. Mater.* **2022**, *34*, e2200705. DOI
85. Hauff E. 2D or not 2D: eliminating interfacial losses in perovskite solar cells. *Chem* **2021**, *7*, 1694-6. DOI
86. Soe, C. M. M.; Nagabhushana, G. P.; Shivaramaiah, R.; et al. Structural and thermodynamic limits of layer thickness in 2D halide perovskites. *Proc. Natl. Acad. Sci. U. S. A.* **2019**, *116*, 58-66. DOI PubMed PMC
87. Duan, J.; Cen, H.; Dai, J.; Wu, Z.; Xi, J. Understand two-dimensional perovskite nanosheets from individual and collective perspectives. *Mater. Today. Electron.* **2024**, *8*, 100097. DOI
88. Cresp, M.; Liu, M.; Rager, M.; Zheng, D.; Pauporté, T. 2D Ruddlesden-Popper versus 2D Dion-Jacobson perovskites: of the importance of determining the “true” average n -value of annealed layers. *Adv. Funct. Mater.* **2025**, *35*, 2413671. DOI
89. Sutanto, A. A.; Caprioglio, P.; Drigo, N.; et al. 2D/3D perovskite engineering eliminates interfacial recombination losses in hybrid perovskite solar cells. *Chem* **2021**, *7*, 1903-16. DOI
90. Wang, T.; Loi, H. L.; Cao, J.; et al. High open circuit voltage over 1 V achieved in tin-based perovskite solar cells with a 2d/3d vertical heterojunction. *Adv. Sci. (Weinh).* **2022**, *9*, e2200242. DOI PubMed PMC
91. Li, H.; Zang, Z.; Wei, Q.; et al. High-member low-dimensional Sn-based perovskite solar cells. *Sci. China. Chem.* **2023**, *66*, 459-65. DOI
92. Kang, Z.; Wang, K.; Zhang, L.; et al. Homogenizing the low-dimensional phases for stable 2D-3D tin perovskite solar cells. *Small* **2024**, *20*, e2402028. DOI
93. Zhang, L.; Huang, C.; Yang, L.; et al. Tactic of A-D-A scheme organic photocatalyst with broad spectral feature of absorption enables photocatalytic performance improvement. *Surf. Interfaces.* **2024**, *48*, 104327. DOI
94. Jokar, E.; Cheng, P.; Lin, C.; Narra, S.; Shahbazi, S.; Wei-guang, D. E. Enhanced performance and stability of 3D/2D tin perovskite solar cells fabricated with a sequential solution deposition. *ACS. Energy. Lett.* **2021**, *6*, 485-92. DOI
95. Sun, M.; Ma, M.; Guo, Y.; et al. Difluorine-substituted molecule-based low-dimensional structure for highly stable tin perovskite solar cells. *Solar. RRL.* **2022**, *6*, 2200672. DOI
96. Li, H.; Xu, Y.; Ramakrishnan, S.; et al. Pseudo-halide anion engineering for efficient quasi-2D Ruddlesden-Popper tin perovskite solar cells. *Cell. Reports. Physical. Science.* **2022**, *3*, 101060. DOI
97. Li, T.; Wang, Y.; Zhu, W.; et al. Synergistic effect of two hydrochlorides resulting in significantly enhanced performance of tin-based perovskite solar cells with 3D to quasi-2D structural transition. *J. Mater. Chem. A.* **2022**, *10*, 14441-50. DOI
98. Gao, W.; Dong, H.; Sun, N.; et al. Chiral cation promoted interfacial charge extraction for efficient tin-based perovskite solar cells. *J. Energy. Chem.* **2022**, *68*, 789-96. DOI
99. Xu, Y.; Jiang, K.; Wang, P.; et al. Highly oriented quasi-2D layered tin halide perovskites with 2-thiopheneethylammonium iodide for efficient and stable tin perovskite solar cells. *New. J. Chem.* **2022**, *46*, 2259-65. DOI
100. Chen, B.; Wang, S.; Zhang, X.; Zhu, W.; Cao, Z.; Hao, F. Reducing the interfacial voltage loss in tin halides perovskite solar cells. *Chem. Eng. J.* **2022**, *445*, 136769. DOI
101. Wang, S.; Wu, C.; Xie, L.; Ding, L.; Hao, F. Pseudohalide-modulated crystallization for efficient quasi-2D tin perovskite solar cells with minimized voltage deficit. *ACS. Materials. Lett.* **2023**, *5*, 936-43. DOI
102. Wang, K.; Yang, P.; Chen, Y.; et al. Rational selection of phenethylammonium salts for 2D/3D tin perovskite solar cells: the halogen ion matters. *ACS. Appl. Energy. Mater.* **2023**, *6*, 10509-17. DOI
103. Zhou, Y.; Yan, D.; Feng, X.; et al. Buried interface modification via guanidine thiocyanate for high-performance lead-free perovskite

- solar cells. *J. Phys. Chem. C*. **2023**, *127*, 1320-5. DOI
104. Yao, H.; Zhu, W.; Hu, J.; et al. Halogen engineering of 2D/3D tin halide perovskite for enhanced structural stability. *Chem. Eng. J.* **2023**, *455*, 140862. DOI
105. Yang, F.; Zhu, R.; Zhang, Z.; et al. High-stable lead-free solar cells achieved by surface reconstruction of quasi-2D tin-based perovskites. *Adv. Mater.* **2024**, *36*, e2308655. DOI
106. Chang, B.; Wang, L.; Li, H.; et al. Phase-pure 2D/3D tin-based perovskite films for solar cells. *ACS. Energy. Lett.* **2024**, *9*, 363-72. DOI
107. Zang, Z.; Ma, M.; Jiang, X.; et al. Efficient quasi-2D tin perovskite solar cells based on mixed monoammonium and diammonium terminal molecules. *Mater. Chem. Front.* **2024**, *8*, 1827-34. DOI
108. Du, F.; Gu, H.; Jiang, W.; et al. Managing crystallization and phase distribution via 2D perovskite seed crystals for 2D-3D tin-based perovskite solar cells. *Adv. Funct. Mater.* **2025**, *35*, 2413281. DOI
109. Pan, H.; Wang, Y.; Zheng, Y.; et al. Phase-pure Ruddlesden-Popper tin halide perovskites for solar energy conversion applications. *J. Mater. Chem. A*. **2024**, *12*, 21008-15. DOI
110. Choi, J.; Kim, J.; Jeong, M.; et al. Molecularly engineered alicyclic organic spacers for 2D/3D Hybrid tin-based perovskite solar cells. *Small* **2024**, *20*, e2405598. DOI PubMed PMC
111. Xu, Y.; Kim, J.; Ramakrishnan, S.; et al. Unraveling the formation mechanisms of highly oriented tin perovskite with a 3D-over-2D heterostructure. *ACS. Energy. Lett.* **2024**, *9*, 4734-45. DOI
112. Kang, Z.; Tong, Y.; Wang, K.; et al. Tailoring low-dimensional phases for improved performance of 2D-3D tin perovskite solar cells. *ACS. Mater. Lett.* **2024**, *6*, 1-9. DOI
113. Feng, G.; Loi, H. L.; Wang, T.; et al. A-site engineering with thiophene-based ammonium for high-efficiency 2D/3D tin halide perovskite solar cells. *Angew. Chem. Int. Ed. Engl.* **2025**, *64*, e202413584. DOI
114. Wang, C.; Zhang, Y.; Gu, F.; et al. Illumination durability and high-efficiency Sn-Based perovskite solar cell under coordinated control of phenylhydrazine and halogen ions. *Matter* **2021**, *4*, 709-21. DOI
115. Wu, T.; Liu, X.; Luo, X.; et al. Lead-free tin perovskite solar cells. *Joule* **2021**, *5*, 863-86. DOI
116. Chen, L.; Fu, S.; Li, Y.; Sun, N.; Yan, Y.; Song, Z. On the durability of tin-containing perovskite solar cells. *Adv. Sci. (Weinh)*. **2024**, *11*, e2304811. DOI PubMed PMC
117. Heo, J. H.; Kim, J.; Kim, H.; Moon, S. H.; Im, S. H.; Hong, K. H. Roles of SnX_2 ($\text{X} = \text{F}, \text{Cl}, \text{Br}$) additives in tin-based halide perovskites toward highly efficient and stable lead-free perovskite solar cells. *J. Phys. Chem. Lett.* **2018**, *9*, 6024-31. DOI
118. Koh, T. M.; Krishnamoorthy, T.; Yantara, N.; et al. Formamidinium tin-based perovskite with low E_g for photovoltaic applications. *J. Mater. Chem. A*. **2015**, *3*, 14996-5000. DOI
119. Liu, G.; Jiang, X.; Feng, W.; et al. Synergic electron and defect compensation minimizes voltage loss in lead-free perovskite solar cells. *Angew. Chem. Int. Ed. Engl.* **2023**, *62*, e202305551. DOI
120. Lai, H.; Olthof, S.; Ren, S.; et al. Unveiling the GeI_2 -assisted oriented growth of perovskite crystallite for high-performance flexible Sn perovskite solar cells. *Energy. Environ. Mater.* **2025**, *8*, e12791. DOI
121. Liu, X.; Wang, Y.; Wu, T.; et al. Efficient and stable tin perovskite solar cells enabled by amorphous-polycrystalline structure. *Nat. Commun.* **2020**, *11*, 2678. DOI PubMed PMC
122. Ryu, D. H.; Kim, J. H.; Obila, J. O.; et al. Erbium chloride-mediated nucleation/crystallization control for high-performance tin-based perovskite solar cells. *EcoMat* **2024**, *6*, e12500. DOI
123. Ng, C. H.; Nishimura, K.; Ito, N.; et al. Role of GeI_2 and SnF_2 additives for SnGe perovskite solar cells. *Nano. Energy*. **2019**, *58*, 130-7. DOI
124. Ito, N.; Kamarudin, M. A.; Hirotsu, D.; et al. Mixed Sn-Ge perovskite for enhanced perovskite solar cell performance in air. *J. Phys. Chem. Lett.* **2018**, *9*, 1682-8. DOI
125. Ng, C. H.; Hamada, K.; Kapil, G.; et al. Reducing trap density and carrier concentration by a Ge additive for an efficient quasi 2D/3D perovskite solar cell. *J. Mater. Chem. A*. **2020**, *8*, 2962-8. DOI
126. Jang, H.; Lim, H. Y.; Yoon, Y. J.; et al. Formate as anti-oxidation additives for Pb-Free FASnI_3 perovskite solar cells. *Solar. RRL*. **2022**, *6*, 2200789. DOI
127. Cao, J.; Tai, Q.; You, P.; et al. Enhanced performance of tin-based perovskite solar cells induced by an ammonium hypophosphite additive. *J. Mater. Chem. A*. **2019**, *7*, 26580-5. DOI
128. Wang, T.; Tai, Q.; Guo, X.; et al. Highly air-stable tin-based perovskite solar cells through grain-surface protection by gallic acid. *ACS. Energy. Lett.* **2020**, *5*, 1741-9. DOI
129. Wang, N.; Zhou, Y.; Ju, M.; et al. Heterojunction-depleted lead-free perovskite solar cells with coarse-grained $\text{B-}\gamma\text{-CsSnI}_3$ thin films. *Adv. Energy. Mater.* **2016**, *6*, 1601130. DOI
130. Chen, Q.; Luo, J.; He, R.; et al. Unveiling roles of tin fluoride additives in high-efficiency low-bandgap mixed tin-lead perovskite solar cells. *Adv. Energy. Mater.* **2021**, *11*, 2101045. DOI
131. Lin, Y.; Shen, L.; Dai, J.; et al. π -Conjugated Lewis base: efficient trap-passivation and charge-extraction for hybrid perovskite solar cells. *Adv. Mater.* **2017**, *29*. DOI
132. Li, W.; Li, J.; Li, J.; Fan, J.; Mai, Y.; Wang, L. Additive-assisted construction of all-inorganic CsSnI_3 mesoscopic perovskite solar cells with superior thermal stability up to 473 K. *J. Mater. Chem. A*. **2016**, *4*, 17104-10. DOI
133. Jung, M.; Ji, S. G.; Kim, G.; Seok, S. I. Perovskite precursor solution chemistry: from fundamentals to photovoltaic applications.

- Chem. Soc. Rev.* **2019**, *48*, 2011-38. DOI
134. Ma, Y.; Liu, C.; Zhang, M.; Mai, Y. Review on the effects of solvent physical properties on the performance of slot-die coated perovskite solar cells. *Surf. Sci. Tech.* **2024**, *2*, 54. DOI
135. Liao, W.; Zhao, D.; Yu, Y.; et al. Lead-free inverted planar formamidinium tin triiodide perovskite solar cells achieving power conversion efficiencies up to 6.22%. *Adv. Mater.* **2016**, *28*, 9333-40. DOI
136. Kayesh, M. E.; Chowdhury, T. H.; Matsuishi, K.; et al. Enhanced photovoltaic performance of FASnI₃-based perovskite solar cells with hydrazinium chloride coadditive. *ACS. Energy. Lett.* **2018**, *3*, 1584-9. DOI
137. He, L.; Gu, H.; Liu, X.; et al. Efficient Anti-solvent-free spin-coated and printed Sn-perovskite solar cells with crystal-based precursor solutions. *Matter* **2020**, *2*, 167-80. DOI
138. Abdel-shakour, M.; Chowdhury, T. H.; Matsuishi, K.; Bedja, I.; Moritomo, Y.; Islam, A. High-efficiency tin halide perovskite solar cells: the chemistry of tin (II) compounds and their interaction with Lewis base additives during perovskite film formation. *Solar. RRL.* **2021**, *5*, 2000606. DOI
139. Duan, C.; Zou, F.; Wen, Q.; et al. A bifunctional carbazide additive for durable CsSnI₃ perovskite solar cells. *Adv. Mater.* **2023**, *35*, e2300503. DOI
140. Deng, L.; Wang, K.; Yang, H.; Yu, H.; Hu, B. Polymer assist crystallization and passivation for enhancements of open-circuit voltage and stability in tin-halide perovskite solar cells. *J. Phys. D: Appl. Phys.* **2018**, *51*, 475102. DOI
141. Ke, W.; Stoumpos, C. C.; Zhu, M.; et al. Enhanced photovoltaic performance and stability with a new type of hollow 3D perovskite {en}FASnI₃. *Sci. Adv.* **2017**, *3*, e1701293. DOI PubMed PMC
142. Khan, N.; Ryu, D. H.; Park, J.; et al. Bromide incorporation enhances vertical orientation of triple organic cation tin-halide perovskites for high-performance lead-free solar cells. *Solar. RRL.* **2022**, *6*, 2200631. DOI
143. Liu, X.; Wu, T.; Chen, J.; et al. Templated growth of FASnI₃ crystals for efficient tin perovskite solar cells. *Energy. Environ. Sci.* **2020**, *13*, 2896-902. DOI
144. Ryu, D. H.; Khan, N.; Park, J. G.; et al. Morphology and performance enhancement through the strong passivation effect of amphoteric ions in tin-based perovskite solar cells. *Small* **2023**, *19*, e2302418. DOI
145. Obila, J. O.; Ryu, D. H.; Oh, S.; et al. Tin-based perovskite solar cells containing a perylene diimide cathode interlayer with a copper top electrode. *ACS. Energy. Lett.* **2024**, *9*, 1090-6. DOI
146. Li, Y.; Wang, Y.; Xu, Z.; Peng, B.; Li, X. Key roles of interfaces in inverted metal-halide perovskite solar cells. *ACS. Nano.* **2024**, *18*, 10688-725. DOI
147. Wang, F.; Jiang, X.; Chen, H.; et al. 2D-quasi-2D-3D hierarchy structure for tin perovskite solar cells with enhanced efficiency and stability. *Joule* **2018**, *2*, 2732-43. DOI
148. Liu, G.; Zhong, Y.; Feng, W.; et al. Multidentate chelation heals structural imperfections for minimized recombination loss in lead-free perovskite solar cells. *Angew. Chem. Int. Ed. Engl.* **2022**, *61*, e202209464. DOI
149. Ma, M.; Jiang, X.; Zang, Z.; et al. Suppressing fluoride segregation for high efficiency tin perovskite solar cells. *Adv. Funct. Materials.* **2024**, *34*, 2407095. DOI
150. Zhao, Z.; Gu, F.; Li, Y.; et al. Mixed-organic-cation tin iodide for lead-free perovskite solar cells with an efficiency of 8.12. *Adv. Sci. (Weinh).* **2017**, *4*, 1700204. DOI PubMed PMC
151. Shao, S.; Liu, J.; Portale, G.; et al. Highly reproducible Sn-based hybrid perovskite solar cells with 9% efficiency. *Adv. Energy. Mater.* **2018**, *8*, 1702019. DOI
152. Jökar, E.; Chien, C. H.; Tsai, C. M.; Fathi, A.; Diau, E. W. Robust tin-based perovskite solar cells with hybrid organic cations to attain efficiency approaching 10. *Adv. Mater.* **2019**, *31*, e1804835. DOI PubMed
153. Ran, C.; Gao, W.; Li, J.; et al. Conjugated organic cations enable efficient self-healing FASnI₃ solar cells. *Joule* **2019**, *3*, 3072-87. DOI
154. Kamarudin, M. A.; Hirotani, D.; Wang, Z.; et al. Suppression of charge carrier recombination in lead-free tin halide perovskite via lewis base post-treatment. *J. Phys. Chem. Lett.* **2019**, *10*, 5277-83. DOI
155. Meng, X.; Wu, T.; Liu, X.; et al. Highly reproducible and efficient FASnI₃ perovskite solar cells fabricated with volatilizable reducing solvent. *J. Phys. Chem. Lett.* **2020**, *11*, 2965-71. DOI
156. Meng, X.; Wang, Y.; Lin, J.; et al. Surface-controlled oriented growth of FASnI₃ crystals for efficient lead-free perovskite solar cells. *Joule* **2020**, *4*, 902-12. DOI
157. Chen, M.; Dong, Q.; Eickemeyer, F. T.; et al. High-performance lead-free solar cells based on tin-halide perovskite thin films functionalized by a divalent organic cation. *ACS. Energy. Lett.* **2020**, *5*, 2223-30. DOI
158. Wang, C.; Gu, F.; Zhao, Z.; et al. Self-repairing tin-based perovskite solar cells with a breakthrough efficiency over 11%. *Adv. Mater.* **2020**, *32*, e1907623. DOI
159. Nakamura, T.; Yakumaru, S.; Truong, M. A.; et al. Sn(IV)-free tin perovskite films realized by in situ Sn(o) nanoparticle treatment of the precursor solution. *Nat. Commun.* **2020**, *11*, 3008. DOI PubMed PMC
160. Jiang, X.; Wang, F.; Wei, Q.; et al. Ultra-high open-circuit voltage of tin perovskite solar cells via an electron transporting layer design. *Nat. Commun.* **2020**, *11*, 1245. DOI PubMed PMC
161. Wang, S.; Yan, L.; Zhu, W.; et al. Suppressing the formation of tin vacancy yields efficient lead-free perovskite solar cells. *Nano. Energy.* **2022**, *99*, 107416. DOI
162. Li, H.; Chang, B.; Wang, L.; et al. Surface reconstruction for tin-based perovskite Solar Cells. *ACS. Energy. Lett.* **2022**, *7*, 3889-99.

[DOI](#)

163. Zhang, Z.; Tian, X.; Wang, C.; et al. Revealing superoxide-induced degradation in lead-free tin perovskite solar cells. *Energy. Environ. Sci.* **2022**, *15*, 5274-83. [DOI](#)
164. Zou, S.; Ren, S.; Jiang, Y.; et al. Efficient environment-friendly lead-free tin perovskite solar cells enabled by incorporating 4-fluorobenzylammonium iodide additives. *Energy. Environ. Mater.* **2023**, *6*, e12465. [DOI](#)
165. Zhu, Z.; Jiang, X.; Yu, D.; Yu, N.; Ning, Z.; Mi, Q. Smooth and compact FASnI₃ films for lead-free perovskite solar cells with over 14% efficiency. *ACS. Energy. Lett.* **2022**, *7*, 2079-83. [DOI](#)
166. Wang, J.; Yang, C.; Chen, H.; et al. Oriented attachment of tin halide perovskites for photovoltaic applications. *ACS. Energy. Lett.* **2023**, *8*, 1590-6. [DOI](#)
167. Zhou, X.; Peng, W.; Liu, Z.; et al. Additive engineering with 2,8-dibromo-dibenzothiophene-*S*,*S*-dioxide enabled tin-based perovskite solar cells with 14.98% power conversion efficiency. *Energy. Environ. Sci.* **2024**, *17*, 2837-44. [DOI](#)